12-1982

Acoustic Streaming as a Mechanism of the Ranque-Hilsch Effect

Joseph Quang Chu
University of Tennessee, Knoxville

To the Graduate Council:

I am submitting herewith a dissertation written by Joseph Quang Chu entitled "Acoustic Streaming as a Mechanism of the Ranque-Hilsch Effect." I have examined the final electronic copy of this dissertation for form and content and recommend that it be accepted in partial fulfillment of the requirements for the degree of Doctor of Philosophy, with a major in Engineering Science.

M. Kurosaka, Major Professor

We have read this dissertation and recommend its acceptance:

Dennis Keefer, K. C. Reddy, J. M. Wu, R. L. Young

Accepted for the Council:
Carolyn R. Hodges

Vice Provost and Dean of the Graduate School

(Original signatures are on file with official student records.)

To the Graduate Council:

I am submitting herewith a dissertation written by Joseph Quang Chu entitled "Acoustic Streaming as a Mechanism of the Ranque-Hilsch Effect." I have examined the final copy of this dissertation for form and content and recommend that it be accepted in partial fulfillment of the requirements for the degree of Doctor of Philosophy, with a major in Engineering Science.

M. Kurosaka, Major Professor

We have read this dissertation
and recommend its acceptance:

Accepted for the Council:

Vice Chancellor
Graduate Studies and Research

ACOUSTIC STREAMING AS A MECHANISM OF THE RANQUE-HILSCH EFFECT

A Dissertation

Presented for the

Doctor of Philosophy

Degree

The University of Tennessee, Knoxville

Joseph Quang Chu

December 1982

DEDICATION

The author dedicates this work to his parents, his brother, Tinh, and his sisters, Nhat and Nguyet, whose sacrifices have provided him with the opportunity and the appreciation of learning.

ACKNOWLEDGEMENTS

The author's deepest thanks are extended to Dr. M. Kurosaka, chairman of the dissertation committee and faculty advisor, for invaluable guidance, support and encouragement throughout the study, without whose help this study could not have been achieved.

Special thanks are also extended to Drs. D. Keefer, K. C. Reddy, J. M. Wu and R. L. Young who have instructed him in the presentation of his dissertation.

The author expresses his gratitude to Mr. J. R. Goodman and Mr. R. D. Fizer, whose help in conducting the experiments in this study can never be overstated.

Acknowledgments are also in order for many of his colleagues for simply being available whenever they could be helpful.

Special thanks are due to Mrs. Sandy Shankle for her excellent typing of the manuscript and for her moral support during the course of this study.

The work is supported by the Air Force Office of Scientific Research, under contract no. F49620-78-C-0045.

ABSTRACT

The Ranque-Hilsch effect or the vortex tube effect is a striking phenomenon observed in swirling flows where air injected tangentially into a single pipe, separates spontaneously into two streams: the colder stream near the tube centerline and the hotter stream near its periphery. In spite of the simplicity of the Ranque-Hilsch tube, the mechanism of the total temperature separation, in the absence of any apparent external work, has not satisfactorily been resolved.

Previously the mechanism has been purported to be due to the turbulent motion. However, if this were the mechanism, one could not explain why, in other turbulent swirling devices, the turbulence does not separate the total temperature in the same manner.

Here experiments are conducted to substantiate a theory that acoustic streaming induced by the pure tone, a spinning wave present in swirling flows, deforms the base Rankine vortex into a forced vortex, resulting in total temperature separation in the radial direction. To verify this, acoustic suppressors of organ pipe type, tuned to the frequency of the vortex whistle, are installed on the Ranque-Hilsch tube. When the pitch of the vortex whistle, which increases as the flow through the tube is increased, hit the tuned frequency, the sound level suddenly tumbled, changing from a shrill whistle to a muffled hiss. At that very instant, the centerline temperature, which had gone down as low as -58^oF immediately leapt upwards to +1^oF corresponding to a sudden drop of temperature separation equal to 59^oF; the temperature near the tube periphery plummeted by 10^oF. This attests the theory that the vortex whistle is indeed the main cause of the Ranque-Hilsch effect.

TABLE OF CONTENTS

LIST OF FIGURES

LIST OF SYMBOLS

C_p	Specific heat at constant pressure
D/Dt	Total derivative with respect to t
dB	Decibel, noise level
f	Frequency
f_e	$-\omega + m\frac{v_e}{R} + kw_e$
f_t	Tuned frequency
k	Wave number in the axial direction
L	The cylinder length
ℓ	Acoustic cavity length
m	Wave number in the tangential direction
p	Pressure of fluid
R	The radius of the cylinder
r	Radius position
R_e	Reynold number based upon L
r_i	Radius at the interface between a forced and free vortex
r_o	Radius of the tube
T^*	Total (stagnation) temperature
t	Time
u	Radial velocity
u'	The linear disturbance of radial velocity
u''	The second order disturbance of radial velocity
$\tilde{u}$	Fourier transform of u'
$V(r_o)$	Base, steady swirl in the tangential direction
v	Angular velocity
v'	The linear disturbance of angular velocity
v''	The second order disturbance of angular velocity
$\tilde{v}$	Fourier transform of v'

v_e	The swirl velocity at the outer edge of the steady boundary layer $v_o(R)$
$\tilde{v}_e$	The amplitude of the unsteady disturbance evaluated at the outer edge of the unsteady boundary layer
w	Axial velocity
w'	The linear disturbance of axial velocity
w''	The second order disturbance of axial velocity
$\tilde{w}$	Fourier transform of w'
w_e	The axial velocity at the outer edge of the steady boundary layer $w_o(R)$
z	Axial position

Greek Letters

α	Frequency parameter relevant to the acoustic streaming near R
β	Unsteady boundary layer characteristic length
Γ	Ωr_i^2
Δ	The difference
δ	The steady boundary layer thickness
δ_u	The unsteady boundary thickness
ϵ	The ratio of steady and unsteady boundary thickness
θ	Angular position
λ	$\frac{r_o}{r_i}$
ρ	Density of fluid
ϕ	Phase lag
Ω	Swirl
ω	Frequency
$\partial/\partial r$	Partial derivative with respect to r

CHAPTER I

INTRODUCTION

In 1931, G. Ranque [1],[1] a French engineer, stumbled upon a new method of separating a gas stream into regions of high and low total temperatures in a vortex flow; this led to the discovery of the so-called vortex tube. The work of Ranque lay undeveloped until Rudolph Hilsch [2] became interested in the vortex tube in relation to his low temperature experiments and published his findings in the mid-forties. Since then, the Ranque-Hilsch tube or vortex tube has been the subject of numerous investigations. These investigations have been involved not only with the Ranque-Hilsch vortex cooling effect per se, but also with the applications of vortex tubes to other purposes such as the containment of gases, with different densities, within the vortex field.

In the Ranque-Hilsch tube or vortex tube, compressed air enters the vortex chamber first, where it is set into a swirling motion by passing through a swirl generator, a stationary ring with tangentially drilled slots. Once within the tube, the swirling air separates by itself into two streams of different total temperatures: the hotter air near the tube periphery and the colder one at the centerline. In the conventional counterflow Ranque-Hilsch

---

[1] Numbers in brackets refer to similarly numbered references in the Bibliography.

tube as shown in Figure 1a, the cold air is extracted from an orifice located near the inlet and the hot air escapes from the other end, where a flow controlling valve is located. The counterflow movement of the air is caused by the difference between the lowered axial pressure at the center and the atmospheric pressure. By adjusting the valve, the temperature and the relative flow rate of the cold and hot streams can be varied. Even by closing the cold end orifice, however, the air flowing only in one direction can still produce the radial separation of the total temperature; this is called uniflow type as illustrated in Figure 1b. Because of its simpler flow pattern, it is convenient to adopt this uniflow type for analysis and experiment throughout the present investigation.

The extreme simplicity of the vortex tube which has no moving parts and the spectacular separation of hot and cold streams suggested that it can be used as an air-operated refrigerator without a motor. As long as the adequate air supply is available, temperature below zero degree can easily be obtained; the tubes are now commercially available and widely used in cooling applications. In spite of its implicity of design and its spectacular effect of producing hot and cold air simultaneously, the mechanism of total temperature separation has remained a subject of controversy. In fact, it has never been fully explained. Consequently, there is a need for fundamental study of the phenomenon with the efforts to clarify the Ranque-Hilsch effect [1],[2]. From a practical point, there exists an increasing demand for better understanding of the temperature separation and the Ranque-Hilsch effect. For example, the Ranque-Hilsch effect may be exploited for turbine cooling in aircraft engines; this opens up a possibility of reducing the specific fuel consumption. Therefore, the understanding of this effect is

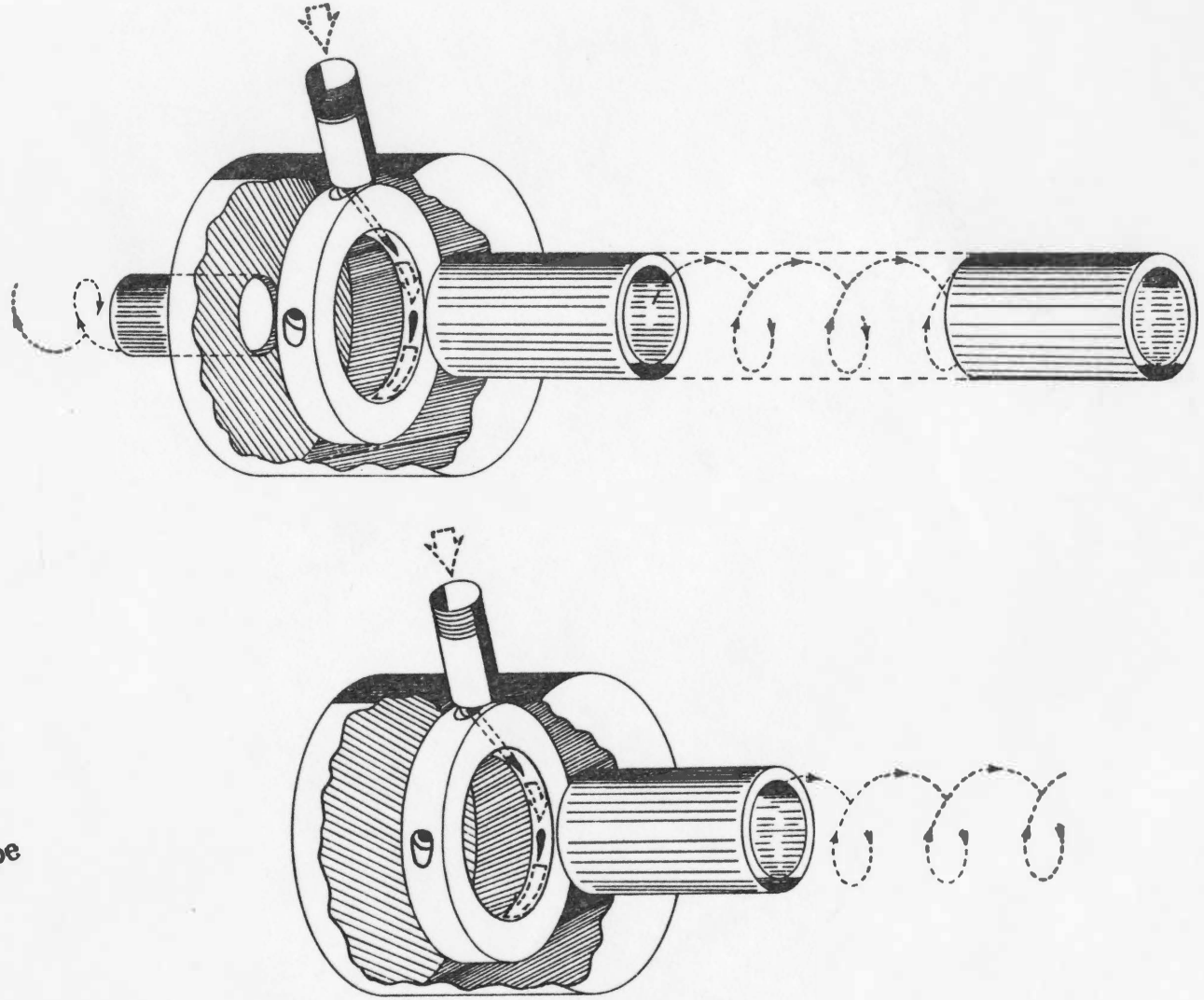

Figure 1. Ranque-Hilsch tube.

important. In the next chapters, a summary of the past hypotheses of the many theoretical and experimental studies will be described, followed by the discussion on a radically new mechanism based upon the phenomenon of acoustic streaming. [This terminology will be defined later.] The objective of present study is directed toward confirmation of the above theory by crucial experiments.

CHAPTER II

PAST THEORIES

Although the radial gradient of static temperature exists in the swirling flow of the Ranque-Hilsch tube, the temperature separation at issue is that of total temperature and not of the static one. Hence, the effect can, by no means, be explained away as due to an isentropic expansion or compression caused by the radial pressure gradient in a vortex. Nor is it due to the Joule-Thomson effect, for the temperature separation observed in the tube is by far the larger; the detailed comparison of the two is given in Appendix A. Nor does the tangential velocity need to exceed the sonic velocity, despite some earlier belief to the contrary. The process defies an immediate explanation, to the extent that some even attributed this, in a lighter vein, to Maxwell's demon coming to life.

As pointed out by Liepmann and Roshko [3], one cannot, in fact, explain this within the framework of steady flow and has to resort to some form of unsteadiness. This is because the material derivative of total temperature is given by

$$C_p \frac{DT^*}{Dt} = \frac{1}{\rho} \frac{\partial p}{\partial t} \tag{2.1}$$

in the absence of any appreciable heat conduction, viscous dissipation and external work. The derivation of the above is given in Appendix B. Were the process steady, the right hand side of the equation would obviously vanish, leading, contrary to what actually happens, to the invariance of the total temperature along any streamline.

Thus the flow must be unsteady. But the crucial issue to be resolved is this: what form of unsteadiness? Either random turbulence or some

orderly disturbance? This is the heart of the matter that has remained unsettled. The oft-expressed turbulent - migration theories [4],[5],[6] attribute the mechanism of the Ranque-Hilsch effect to turbulent energy transfer in general and the random migration of flow in the radial direction in particular. Deissler and Perlmutter [5], Linderstrom-Lang [6] stated that the total temperature separation in the vortex tube depends on the contributions of turbulent shear work done by Reynolds stress corresponding to radial migration of tangential velocity and of turbulent heat transfer due to radial migration of thermal energy under pressure gradients (by expansion and contraction of eddies).

The experimental evidences will now be discussed. Hartnett and Eckert [7], Keyes [8], Lay [9], Linderstrom-Lang [6], Reynolds [10], Savino and Ragsdale [11], Scheller and Brown [12], Takahama [13], Bruun [14] and Sibulkin [15] have measured internal flows in the Ranque-Hilsch tube. In most of these reported studies, total temperatures, velocities or turbulence in the Ranque-Hilsch tube were taken at optimum cooling conditions. There, the forced vortex is always found at any swirl and it forms immediately near the tangential inlets. It occupies the entire cross section (except near the tube wall boundary layer) and remains so from the entrance to the exit. At this condition, no vestige of a free vortex is found even in the inlet. All the experimental data show that the separation of the total temperature between hot and cold streams is maximum right near the inlet. As air flows toward the exit, the degree of total temperature separation decreases in the axial direction due to dissipative effect. The turbulence level in the Ranque-Hilsch tube was measured by Sibulkin to be 3—7% [15].

The turbulent migration theories assert that turbulent energy transfer is necessarily involved with the temperature separation of the Ranque-Hilsch effect. If turbulence is the main catalytic agent, the theories fail to explain the following: why in the particular case of the Ranque-Hilsch tube turbulent migration can abruptly lead to a forced vortex and the sudden separation of total temperature (as observed by Hartnett and Eckert and others) while, in other swirling flow devices [16] with the same tangential injection and turbulence level as for the case of Ranque-Hilsch tube, it can still retain a free vortex (plus forced vortex type in the center core) and virtually uniform total temperature in the radial direction. The other theories proposed by Sibulkin [15], Scheper [17] appear to be open to equally serious objections.

The experimental evidence on some aircraft engine test rig to be presented shortly seems to point toward a pure tone or periodic disturbance as an agent of the Ranque-Hilsch effect.

In the literature on the Ranque-Hilsch tube, the presence of intense periodic disturbances is widely observed. Hilsch [2], McGee [18], Savino and Ragsdale [11], Kendall [19], Ragsdale [20], and Syred and Beer [21] recounted, in one way or the other, the disturbances of pure tone type or the whistle. Sprenger [22], [23] even suggested that the mechanism of total temperature separation accomplished within the Ranque-Hilsch tube may be analogous to the one of the resonance tube, which is attributed to organized unsteadiness. In fact, Savino and Ragsdale [11] recorded an incident where a loud screaming noise was accompanied by $10 - 20^{o}F$ change in total temperature, but they did not give any explanation on its mechanism.

CHAPTER III

BACKGROUND TO THE PRESENT THEORY

Of late, a striking phenomenon has unexpectedly presented itself in the aircraft engine test rig – the annular cascade – built for the transonic flutter testing of the blades in the non-rotating environment [24],[25],[26]. As a whole, it is in the shape of a stationary annular duct formed between inner and outer casings; swirling air created by the variable stator vanes enters the test section, where the test cascade airfoils are nominally mounted on the outer casings. The whistle unexpectedly occurred in the check-out phase of the test rig prior to the flutter experiment and its presence was detected even after the removal of the airfoils; the frequency of the whistle was found to increase almost proportionally to the flow rate or swirl. The dynamic fluctuation was so intense as to pose a serious threat to the subsequent test of bladings. Hence, dynamic measurements of the vortex whistle have been carried out to seek means to suppress the whistle. Based upon this, the duct was installed with acoustic suppressors and the unacceptable dynamic flow disturbance was finally removed. Ever since, the vehicle has successfully been used for aeroelastic purposes and served to identify and establish important aspects of transonic flutter [25], the details are, however, outside the present interest. What interests us is the phenomenon observed while the vortex whistle is still present.

In addition to the increase of frequency proportional to the flow rate, the data, taken at a time when nothing lays in the flow path, reveals the following unexpected change in the steady or time averaged flow field.

When the whistle was inaudible, the steady state tangential velocity distribution in the radial direction was in the form of free vortex; the steady state temperature was uniform. However, when the whistle became so intense, the radial profile transformed from a free vortex into a forced vortex; furthermore, the total temperature initially uniform at the inlet and equal to 97^oF, spontaneously separated into hotter stream of about 118^oF near the outer wall and colder one of 83^oF near the inner wall, with the difference as distinct as 35^oF. The latter reminds us of the Ranque-Hilsch effect [1],[2]. Concurrently with this, the total pressure near the outer wall exceed its upstream value, while the one near the inner wall became less. Upon the installation of the acoustic suppressors, which had succeeded in eliminating the vortex whistle, the deformation in the radial profiles of velocity temperature and pressure vanished.

Besides these observations recorded in the annular cascade, additional similar incidents were observed in the other test rig of Detroit Diesel Allison, Indianapolis, Indiana [27]. The whistle, apparently induced by swirl created downstream of inlet guide vanes, was detected beyond a certain flow rate; corresponding to the initiation of the sound, the exhaust became noticeably warm when touched by hand, while the formation of ice was detected on the surface of the back plate at a location corresponding to the centerline of the pipe. At the same time, the total pressure, measured at a point near the periphery of the exhaust pipe, reached 16 psia while the pressure of the upstream incoming air was 14.2 psia; therefore, the downstream total pressure exceeds its upstream value by 12.7 percent. Furthermore, the maximum Mach number and mass flow was considerably lower than expected. The installation of acoustic suppressors eliminated these effects

as in the case of the annular cascade; the downstream total pressure was decreased to 13.2 psia, the temperature separation disappeared and both the maximum Mach number and flow increased by 30 percent.

These experiences obtained in the aircraft engines suggest that an organized disturbance (a pure tone or the so-called vortex whistle) rather than the turbulence, causes the Ranque-Hilsch effect. The phenomenon where a pure tone or a.c. disturbance modify the steady or d.c. base flow is, in general, called acoustic streaming [28]. The thesis is that acoustic streaming induced by the vortex whistle is a mechanism of the Ranque-Hilsch effect. The vortex whistle and acoustic streaming will be elaborated further in the following sections.

a. Vortex Whistle

The vortex whistle or the pure tone noise existing in any swirling flow, emerges out of the selective amplification of background disturbances and it grows in intensity by drawing energy from the flow itself. As it turns out, the vortex whistle is an inviscid, inertial wave, whose frequency increases proportionally to swirl and is determined primarily by the profile and intensity of swirl, wave numbers and tube radius.

The tone emanates even out of a swirl created by the tangential injection into a stationary cylinder, including the Ranque-Hilsch tube. Historically, Vonnegut [29],[30] discovered the presence of a pure tone with its frequency proportional to swirl when experimenting to exploit the Ranque-Hilsch effect. The continuous change in the frequency enables one to play musical tones in a simple manner by varying the blowing pressure by mouth. It was Vonnegut [29], who named the sound as the vortex whistle. The linear accuracy that, by creating swirl and measuring its frequency, it can

be used either as a sensor of aircraft frequency, it can be used either as a sensor of aircraft speed [31] or a flowmeter [32], provided that in the latter the ratio of swirl to axial velocity is made to remain constant.

b. Acoustic Streaming

How can such a phenomenon as acoustic streaming, the modification of the base, d.c. component of flow by a.c. disturbances, happen? The root of this lies in the nonlinear convection term in the equation of motion.

Within the framework of more familiar linear acoustics, where the amplitude of disturbances remains small, the a.c. disturbance expressed for instance, as $\cos\omega t$, does not modify the base steady state, since the temporal average of $\cos\omega t$ over a period of oscillation is obviously zero. Once the amplitude of a.c. component increases, however, the nonlinearity of the convective term generates a waveform, consisting of the product of linear waves, like $\cos^2\omega t$; its temporal average being non-zero, the unsteady disturbance now induces an additional steady component and modifies the base steady state. To be more precise, the presence of viscous terms is as equally important as the convection terms [33] for acoustic streaming. The importance of both effects is described mathematically in Appendix C.

Acoustic streaming can be demonstrated not only in assorted laboratory experiments using a vibrating diaphragm [34], cylinder [35] and the like, but also it has been suggested as a possible explanation ranging from the roll torque effects of rocket motors in flight [36],[37] to the blood flow phenomena in the coronary arteries [38].

CHAPTER IV

MATHEMATICAL ANALYSIS OF THE PROBLEM

By posing a model problem simulating the vortex tube of uniflow type, the effect of periodic disturbances in a swirling flow within a single tube has been recently studied. Details on the mathematical analysis are available in "Acoustic Streaming in Swirling Flows and the Ranque-Hilsch Effect" by M. Kurosaka (to appear in Journal of Fluid Mechanics) as reported in Reference [39], but for completeness a summary will be given here.

First, consider the full compressible unsteady Navier-Stokes equations in cylindrical coordinates. The streaming effects are of primary interest. Acoustic streaming is an induced steady or added d.c. component. Thus the flow at any point consists of three parts: the steady part, the a.c. components of the unsteady disturbances and their d.c. components or streaming. The sum of the steady part and streaming is the total d.c. component.

The base steady flow is taken to be a helix. Its axial velocity is constant and swirl is assumed to be a Rankine vortex, a combination of a forced vortex occupying a core and a free vortex elsewhere. In order to obtain the leading terms of acoustic streaming, all the flow variables are expanded in power series of $\alpha, \beta, \epsilon (<< 1)$, which are given by

$$\alpha = \frac{\tilde{v}_e}{f_e R}$$

$$\beta = \frac{\delta_u}{R} = \left[\frac{\nu}{|f_e|}\right]^{\frac{1}{2}} \frac{1}{R} \tag{4.1}$$

$$\epsilon = \frac{\delta}{\delta_u} = \frac{L}{\beta R R_e^{\frac{1}{2}}}$$

where

$f_e = -\omega + m\frac{v_e}{R} + kw_e$

v_e = the swirl velocity at the outer edge of the steady boundary layer $v_o(R)$

$\tilde{v}_e$ = the amplitude of the unsteady disturbance evaluated at the outer edge of the unsteady boundary layer.

R = the radius of the cylinder

δ = the steady boundary layer thickness, $= R_e^{\frac{1}{2}}$

δ_u = the unsteady boundary layer thickness

R_e = Reynold number based upon L

L = the cylinder length

ω = frequency

w_e = the axial velocity at the outer edge of the steady boundary layer $w_o(R)$

m = wave number in the circumferential direction

k = wave number in the axial direction

Physically, α is a frequency parameter relevant to the acoustic streaming near R; β unsteady boundary layer characteristic length; ϵ the ratio of steady and unsteady boundary layer thickness.

As regards δ_u and β, the magnitude of f_e is needed, for its sign can and does switch, depending upon the relative magnitudes of ω, v_e and w_e. Note that as the steady flow varies, the unsteady boundary layer thickness δ_u can change, even for a given frequency. For example, δ_u may increase when f_e is decreased by an increase in v_e only. What this implies is, in effect, that the unsteady boundary layer can become thicker than the steady one, particularly at high Reynold number. Physically, these amount to the following: the amplitude of unsteady disturbances is small and compared with the length scale of the cylinder radius, the unsteady boundary layer

is thin. Within the unsteady boundary layer, an even thinner steady boundary layer is embedded.

It can be shown that the leading term of acoustic streaming is $O(\alpha)$; then, as far as the leading term is concerned, terms of $O(\beta)$, $O(\epsilon)$ and other higher-order corrections can be neglected. Thus the flow variables can be rewritten in the form:

$$\begin{aligned} u &= u' + u'' + \cdots \\ v &= v_e + v' + v'' + \cdots \\ w &= w_e + w' + w'' + \cdots \end{aligned} \tag{4.2}$$

where v_e, w_e are constant; u', v', w' correspond to the linear disturbance; u'', v'', w'' correspond to the second order disturbance,

and

$$O\left(\frac{u'}{\tilde{v}_e}\right) = O\left(\frac{v'}{\tilde{v}_e}\right) = O\left(\frac{w'}{\tilde{v}_e}\right) = 1$$

$$O\left(\frac{u''}{\tilde{v}_e}\right) = O\left(\frac{v''}{\tilde{v}_e}\right) = O\left(\frac{w''}{\tilde{v}_e}\right) = \alpha$$

Substituting the above expressions into the Navier-Stokes equations yields a set of equations appropriate for each order. Suppose the linearized forms of the periodic disturbance have solutions of the form

$$\begin{aligned} u' &= \tilde{u}(r)\exp(i(m\theta + kz - \omega t)) \\ v' &= \tilde{v}(r)\exp(i(m\theta + kz - \omega t)) \\ w' &= \tilde{w}(r)\exp(i(m\theta + kz - \omega t)) \end{aligned} \tag{4.3}$$

where $\tilde{u}, \tilde{v}, \tilde{w}$ are the Fourier transforms of u', v', w' in m and k. Physically, these represent helically advancing waves. Then, over any cylindrical surface drawn within the pipe, the pattern of double helixes can be visualized: one corresponding to the aforementioned steady vortex (Figure 2a), the other to the unsteady wave which, for example, represents the trajectory

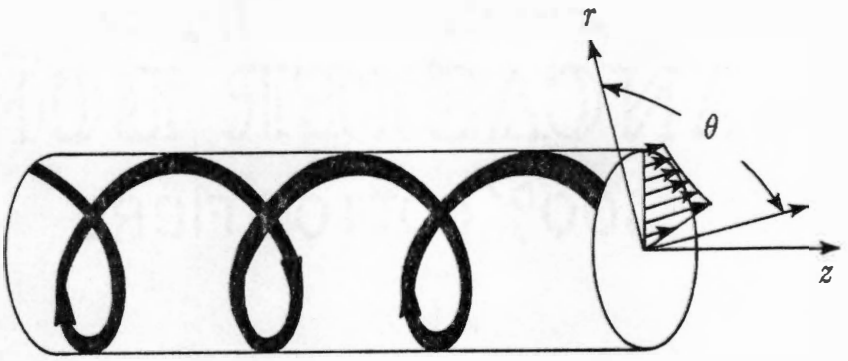

(a) steady helix

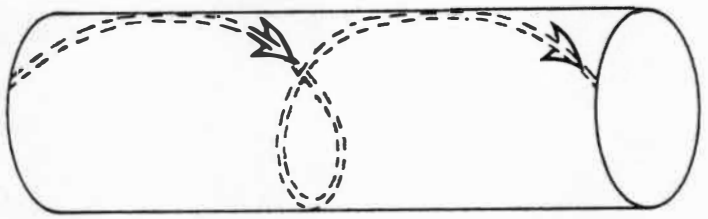

(b) helically advancing unsteady wave

Figure 2 Definition sketch and helical pattern.

of its crest (Figure 2b). In reality, there are of course, an infinite number of such pairs of double helixes, each starting from any given point on the periphery of the imaginary cylindrical surface. The pitches of the double helixes are different.

Near the tube surface, the local structure of the flow divides radially into two regions: (a) a thin annular viscous region adherent to the tube periphery, corresponding to the steady and unsteady boundary layer and (b) the larger inviscid core outside of it. Before unsteady disturbances set up, the steady boundary layer is rotationally symmetric and develops in the z - direction. Once the unsteady disturbances arise, the unsteady boundary layer emerges. In accordance with the preceding discussions and subject to the restrictions imposed by the condition $\alpha, \beta, \epsilon \ll 1$, the thickness of steady boundary layer is negligible in comparison with the unsteady boundary layer thickness. Hence the unsteady boundary layer virtually dominates the entire annular viscous region near the tube periphery; the inviscid core surrounds this viscous layer.

The sequential steps to determine the waves in the two regions are as follows: linearized disturbances in the inviscid core determines both the frequency as the eigenvalue and the corresponding linear disturbance in the unsteady viscous layer; this in turn, brings acoustic streaming into being out of the second order disturbances in the viscous layer; this acoustic streaming drives its counterpart in the inviscid core.

Amid the analytical conclusions of Reference [39], three prominent results are presented here: (a) frequency ω, (b) the form of the second order waves and (c) the tangential acoustic streaming at the outer edge of the unsteady viscous layer.

a. Frequency

As mentioned, for a model "inviscid" base steady velocity profile corresponding to a Ranque-Hilsch tube of uniflow type, a Rankine vortex within a single pipe, described below, is taken:

$$\begin{aligned} V(r) &= \Omega r\,, \quad o < r < r_i \\ V(r) &= \frac{\Gamma}{r}\,, \quad r_i < r < r_o \end{aligned} \tag{4.4}$$

where $\Gamma = \Omega r_i^2$, r_i denotes the radius at the interface between a forced and free vortex, r_o the radius of the tube. The boundary condition of zero normal velocity suffices to fix ω. Expanding the dependent variables in power series of Ω, a solution for eigenvalue ω can be obtained in closed form, which, though approximate, is valid over a wide range of swirl. In regard to the lowest eigenvalue, the frequency - swirl relationship is determined as

$$\omega = (m - 1 + \lambda^{-2m})\Omega \tag{4.5}$$

where $\lambda = \frac{r_o}{r_i}$.

This shows that the frequency is proportional to the swirl – a key feature of the vortex whistle in a single pipe discovered by Vonnegut [29] and confirmed by Chanaud [40],[41]. For the special case of $m = 1$, the first tangential mode and $k = 0$, this reduces to

$$\omega = \frac{V(r_o)}{r_o} \tag{4.6}$$

where $V(r_o)$ is the base, steady swirl at the tube periphery. Since the frequency is independent of the physical properties of the fluid, the above expressions are also applicable to incompressible fluid. It can also be directly verified by examining the incompressible solution obtained by Kelvin [42].

The details of this are given in Appendix D. This explains the reason why in Vonnegut's vortex whistle [29], the data of frequency - swirl measured for both air and water is found to be on the same curve.

b. The Form of the Second Order Waves

The linear disturbance within the viscous layer can be expressed in such a form as

$$\begin{aligned} u' &= \tilde{u}(r)\cos(m\theta + kz - \omega t + \phi_o(r)) \\ v' &= \tilde{v}(r)\cos(m\theta + kz - \omega t + \phi_1(r)) \end{aligned} \tag{4.7}$$

where $\tilde{u}(r)$ and $\tilde{v}(r)$ are the amplitudes of the disturbances; ϕ_o and ϕ_1 the phase lags.

Then, among the second order disturbance equation in the tangential direction, there exists, for example, a term like

$$\begin{aligned} \frac{\partial}{\partial r}(u'v') = \frac{\partial}{\partial r}\left[\frac{1}{2}\tilde{u}(r)\tilde{v}(r)\cos(\phi_o - \phi_1)\right] \\ + \cos(2m\theta + 2kz - 2\omega t)\frac{\partial}{\partial r}\left[\frac{1}{2}\tilde{u}(r)\tilde{v}(r)\cos(\phi_o + \phi_1)\right] \\ - \sin(2m\theta + 2kz - 2\omega t)\frac{\partial}{\partial r}\left[\frac{1}{2}\tilde{u}(r)\tilde{v}(r)\sin(\phi_o + \phi_1)\right] \end{aligned} \tag{4.8}$$

The second order disturbance in the tangential direction, v'', comprises above terms. Specifically here, one notes that, first the d.c. component or acoustic streaming emerges in the first term, while the a.c. component of the second order waves appears in the second and third terms, where its argument becomes $2m\theta + 2kz - 2\omega t$; that is, compared to the linear disturbance of Eq. (4.7), not only the frequency gets double from ω, but also the wave number from m to $2m, k$ to $2k$.

It should be noted that this doubling of frequency and wave numbers in the second order waves takes place in the inviscid core as well as in the boundary layer.

c. Tangential Acoustic Streaming

For $m = 1$ and regardless whatever λ may be, the temporal average of v'' at the outer edge of the viscous layer is predicted to become infinitely large; in reality, this, of course, implies that considerable magnitude of acoustic streaming near the tube periphery is induced and it adds to and increases the steady swirl there. Thus tangential streaming adds to tangential velocity near the tube periphery, and converts the original Rankine vortex into a forced vortex type as shown in Figure 3. Even disregarding the effect of the static temperature gradient, the deformed base swirl by acoustic streaming tends to separate the initially uniform total temperature into the hotter stream near the tube periphery and the colder one near the center core. This is none other than the Ranque-Hilsch effect itself.

In the inviscid core the static temperature is determined by the total swirl. From the energy equation, if one assumes that the leading term of the outer expansion of entropy remains constant everywhere, the static temperature for a forced vortex with sufficiently higher speed close to the tube periphery is lower than that of the Rankine vortex, provided that the temperature near the tube wall remains the same. Its derivation is given in Appendix E. This difference in static temperature further separates the total temperature.

The above resonance-like streaming is predicted to occur regardless of the magnitude of the base swirl, or, of the axial position within the tube, even near the inlet. These fit in well with the previous observations: as mentioned, detailed measurements of the internal flow in the Ranque-Hilsch tube, taken at the conditions of optimum cooling, indeed show that in every instance a forced vortex is formed immediately near the entrance

a. Rankine vortex in the absence of unsteady disturbance

b. Forced vortex with acoustic streaming

Figure 3. Deformation of swirl by acoustic streaming.

to the tube, even at a location as practically close as possible to the inlet nozzle. The forced vortex occupies almost the entire cross section, except of course in the neighborhood of the boundary layer on the tube periphery and remains so from the entrance to the exit. Also right at the tube entrance, the radial separation of total temperature induced by the formation of forced vortex, is also found by many experimenters.

Recall once again that this acoustic streaming for $m = 1$ should be accompanied by its a.c. counterpart, with its frequency equal to 2ω and the tangential wave number m equal to 2.

CHAPTER V

EXPERIMENTAL RESULTS AND DISCUSSIONS

In order to obtain experimental proof of the important role played by acoustic streaming in the Ranque-Hilsch effect, an experiment was conducted to verify that the total temperature separation in the radial direction can be reduced by the suppression of the vortex whistle.

As an initial test rig, a commercially available counterflow Ranque-Hilsch tube (Vortec Corporation, Model 328-50), like the one shown in Figure 1a, (Page 3) is obtained: a thin walled cylindrical tube of 0.6875 inches in diameter and 9 inches in length is mounted on the axis of the vortex chamber where a stationary swirl generator with four tangentially drilled slots inclined 72^o from the radial direction is installed. The compressed air from a surge tank enters the vortex chamber through tangential nozzles and then separates into two streams of different total temperature: the hotter air near the tube periphery discharges from one end, the flow rate is controlled by a flow globe valve, while the colder air at the center is extracted from a diaphragm at the other end. Preliminary tests of this vortex tube reveal the following: the air separates into hot and cold streams, each discharges out of its corresponding opening and a pure tone or vortex whistle, whose frequency is proportional to the flow rate or swirl, is dominant over the entire frequency spectra.

To make comparison with the analytical model, a number of modifications should be made. First, the cold end in the vortex chamber is blocked with a Teflon plug to change the present vortex tube to a uniflow type, like the one shown in Figure 1b (Page 3). Now the air flows only in one

direction toward the exhaust and the total temperature separation in the radial direction is still preserved. Because of the simplicity of the flow within the uniflow type, it was used as a basic arrangement throughout the investigation. Figure 4 shows a schematic view of test apparatus. Two important parameters in the present tests of the vortex tube are a pure tone sound and temperature.

In general, it is found easier to use the shorter tube for the subsequent acoustic suppression. Hence, the initial tube is replaced with a shorter tube of 1.65 inches in length; the total temperature separation capability is not impaired. With the length of the tube thus shortened, it is observed that the presence of the controlling globe valve at the exhaust end seriously affects the intensity of the vortex whistle. At the same time, a provision of some form of block at the exhaust is required to prevent entrainment of the ambient air into the tube, which otherwise would occur due to the lowered pressure at the core of the vortex. To meet these conflicting requirements, several configurations of conical shapes are tried; among these, a shape shown in Figure 4 is finally selected. In the experiment to be described here, the tip of the entrainment block is always placed in the exit plane of the exhaust.

As shown in Figure 5, the supply air for the vortex tube passes through a series of pressure regulators that served to steady the flow. It then passes through an ASME orifice flow meter. Eighty diameters downstream of the meter a sound muffler is placed to reduce any sound transmission and to further steady the flow. The 0.250 inch pipe downstream of the muffler leads to the tangential inlet nozzles. Two thermocouples are installed:

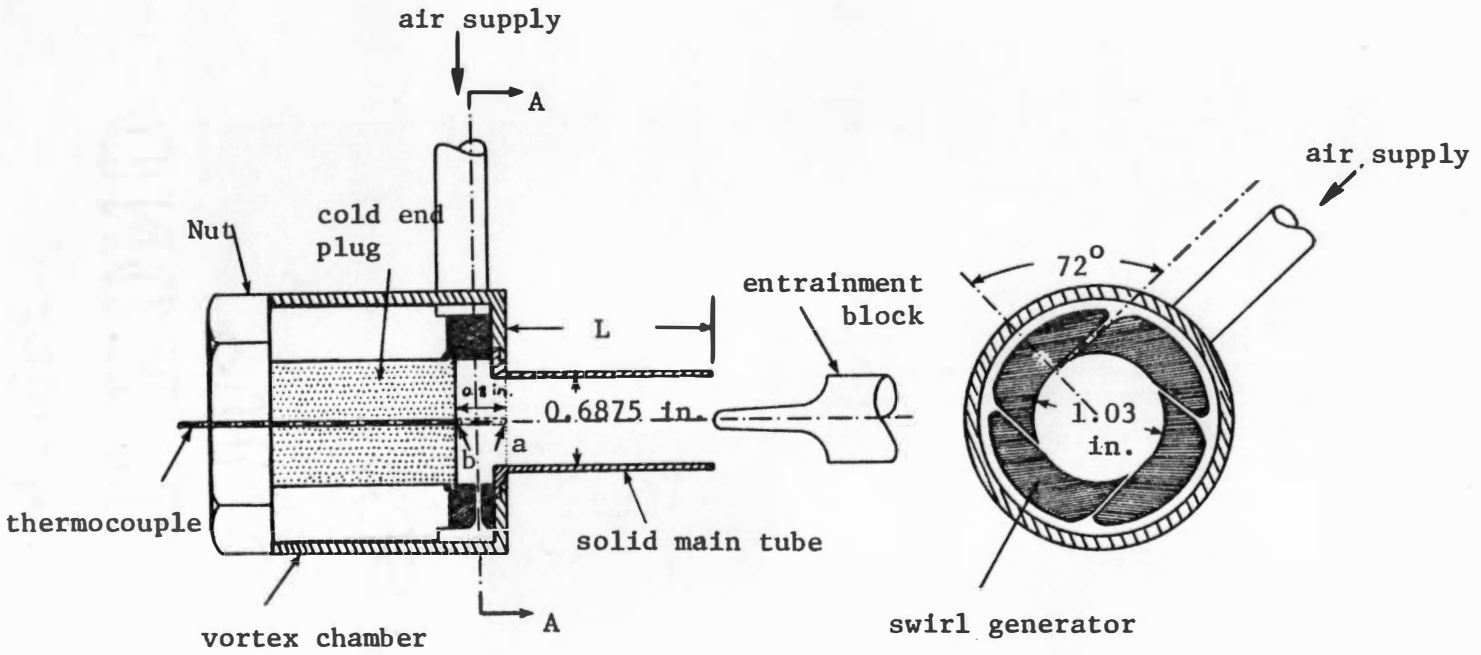

Figure 4. Layout of test rig: solid main tube.

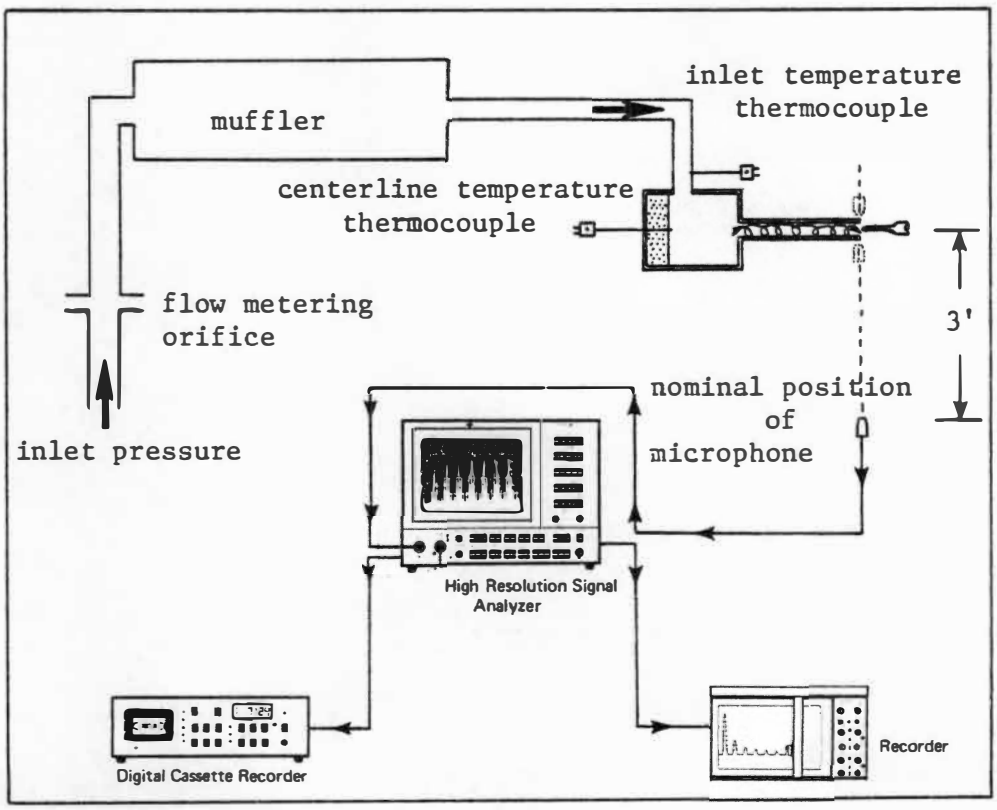

Figure 5. Entire test assembly.

(1) a 0.125 inch Chromel-Alumel thermocouple placed just upstream of the vortex chamber to monitor the inlet temperature, (2) and for centerline temperature, a 0.0625 inch thermocouple inserted through the cold end Teflon plug. A one-quarter inch free-field condenser microphone is mounted on a traversing stand perpendicular to the flow axis centerline; it is positioned at a nominal distance of 3 feet away from the test rig. Its signals are passed through a preamplifier to a FFT High Resolution Signal Analyzer and its output of displayed data can be transmitted to an x-y recorder or stored in a Digital Cassette Recorder.

a. Solid Pipe

As a measurement of temperature separation, ΔT^* is defined as

$$\Delta T^* = T^*\text{inlet} - T^*\text{centerline} \tag{5.1}$$

The data for ΔT^* at two locations and the inlet temperature are shown in Figure 6a: one at the position where the thermocouple is flush with the cold end plug (position b of Figure 4) and the other at 0.8 inches away from it (position a), which corresponds to the cold spot. As one can see, the presence of the cold spot near the entrance to the tube agrees with the finding of others. As the inlet pressure goes up, the temperature separation continuously increases; for instance, at the pressure of 40 psig $\Delta T^* = 114^oF$, corresponding to T^* centerline $= -52^o$ (position a). As discussed earlier, if the acoustic streaming is indeed a mechanism, the total temperature separation should occur near the tube entrance and even at low inlet pressure. Note that the inlet temperature remains nearly constant.

Figure 6b is an example of a narrow band frequency spectrum: the conspicuous peaks, corresponding to the fundamental frequency $f(f = \omega/2\pi)$

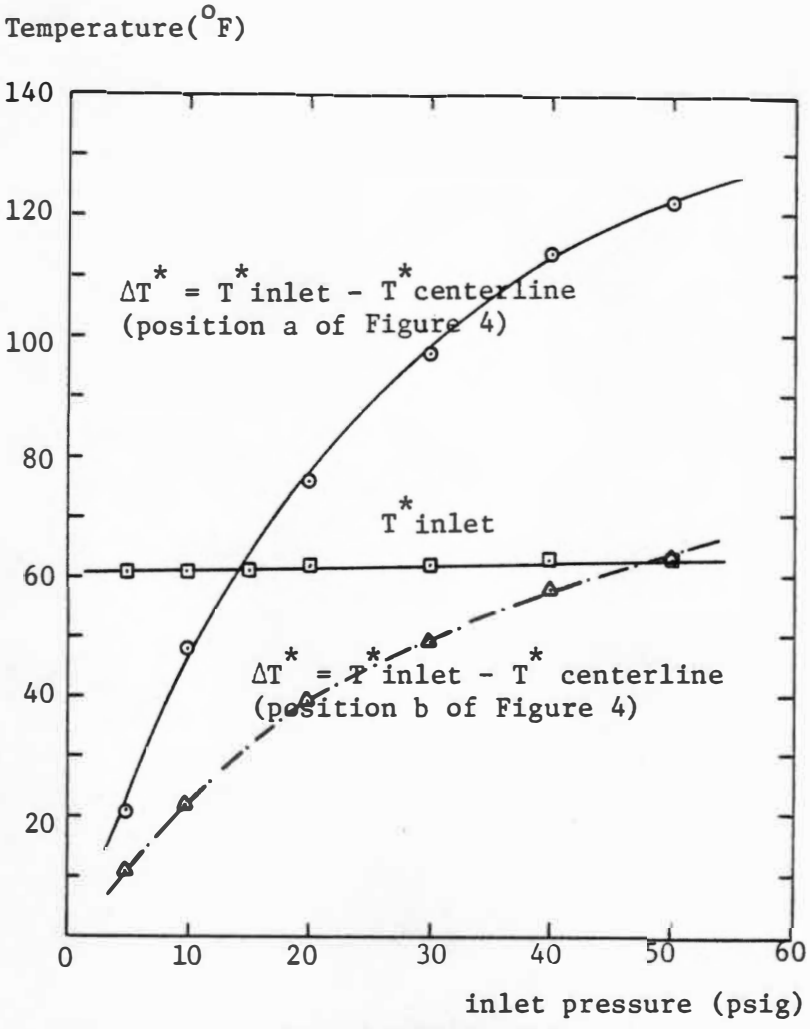

a. Measured temperature for solid pipe

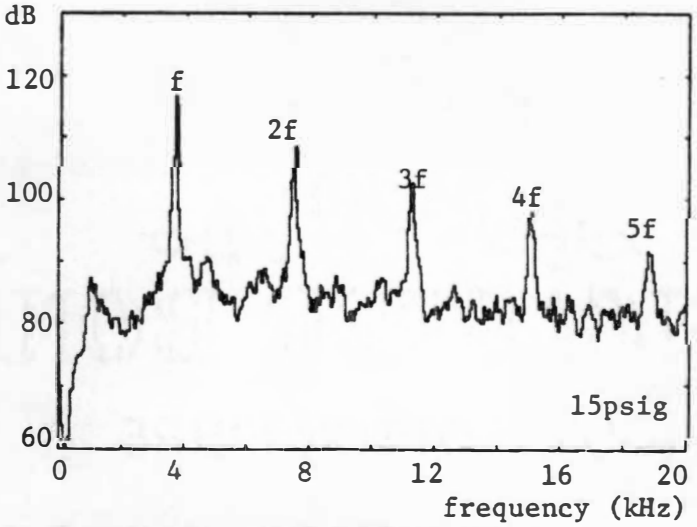

b. Frequency spectrum for solid pipe

Figure 6. Data for solid main pipe.

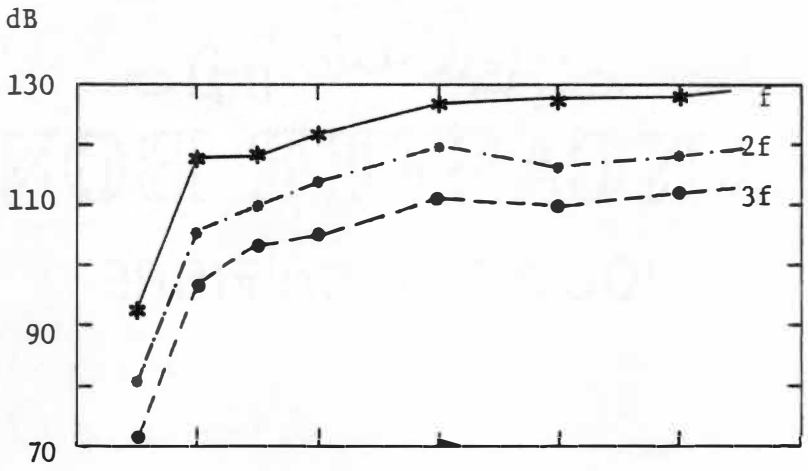

c. Sound level for solid pipe

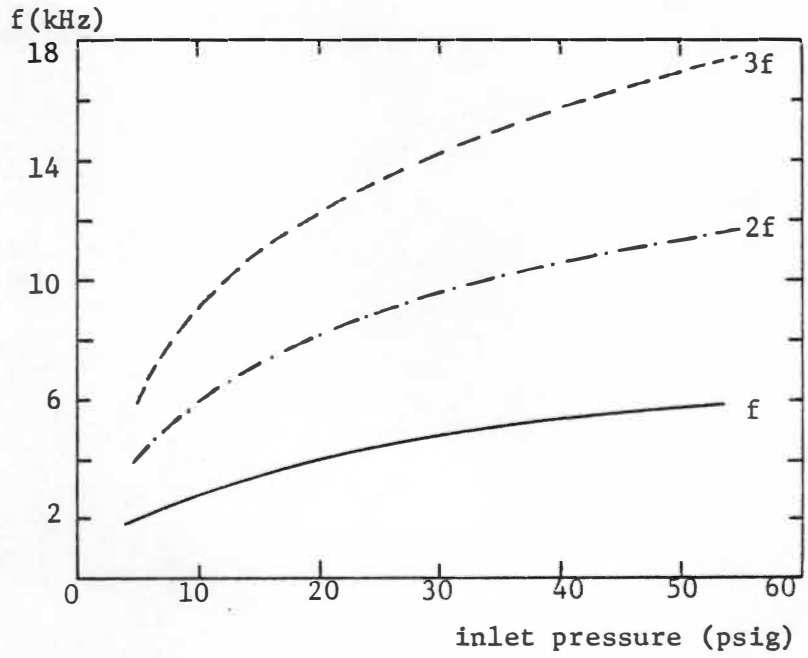

d. Frequency for solid pipe

Figure 6. (continued)

and its higher harmonics up to the fifth soar overshadow the broadband noise. The dependence of the sound level of the vortex whistle due to the inlet pressure is shown in Figure 6c; the increase of the frequency can be seen in Figure 6d.

The tangential wave number of the pure tone corresponding to the fundamental frequency f is found, by the method to be described immediately, to be that of the first circumferential wave, $m = 1$; corresponding to $2f$, $m = 2$. This doubling of the wave number when the frequency is doubled reveals that the second harmonic corresponds to the second order waves, as predicted by the analysis.

The values of m are determined by placing two microphones at the same axial location near the exhaust end of the solid tube and by measuring the phase difference at different, relative position in the tangential direction. Its phase difference can be obtained directly by using a phase meter or by displacing their output signals on the dual-beam oscilloscope as Lissajous figures, the details of the latter method are described below.

By filtering the disturbance, except for the fundamental signal with the frequency f, and by measuring it at a fixed axial position of exit plane, which one can take $z = 0$ without loss of generality, the waveform for $m = 1$ appears as

$$\cos(\theta - \omega t)$$

If a microphone X is placed at $\theta = 0$ (Figure 7a) the signal represents $x = \cos \omega t$; a microphone Y placed at $\theta = 180^o$, the signal is $y = -\cos \omega t$. Therefore, once t is eliminated, $x = -y$. That is, for the first tangential mode of the trajectory of two signals in $x - y$ plane should be a straight line segment inclined 45^o, lying in the second and the fourth quadrant, in

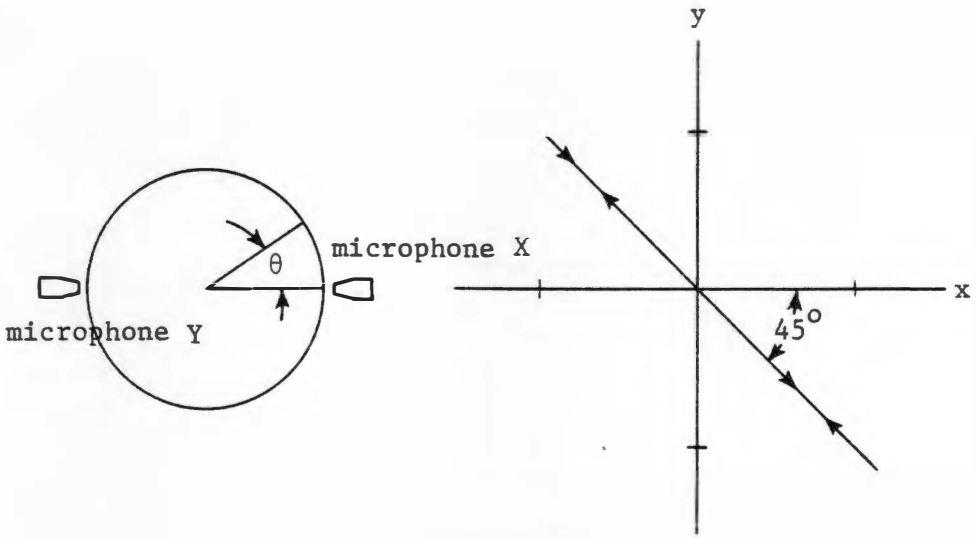

a. Trajectory of signals received by two microphones placed 180° apart

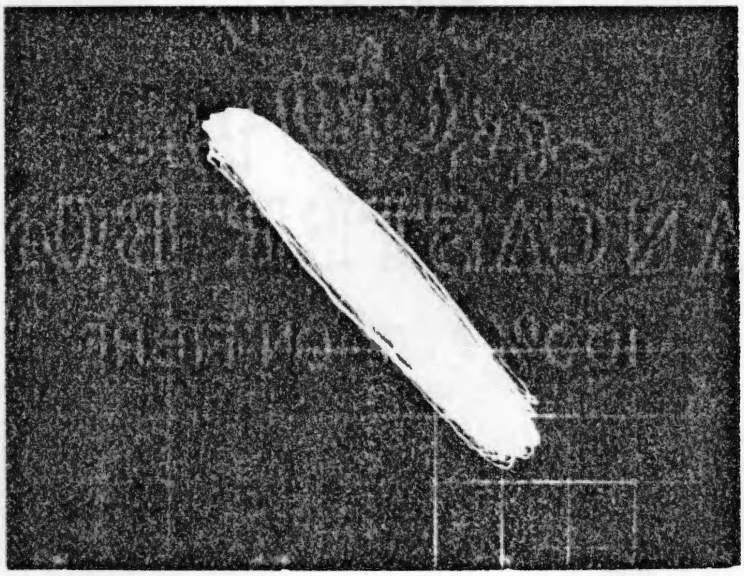

b. Lissajous figure for 180° microphone arrangement

Figure 7. Tangential wave number trajectory for 180° microphone arrangement.

fact, the Lissajous figure displayed on a dual-beam osilloscope appears like so, as seen from Figure 7b. Now is the Y microphone moves to the $\theta = 90^o$ position, Figure 8a, its signal appears to be $y = \sin \omega t$, while the x signal still remains $x = \cos \omega t$; since $x^2 + y^2 = 1$, the trajectory should now be a circle and the Lissajous displayed in Figure 8b again appears so. The analysis predicts that for $m = 1$ wave, acoustic streaming near the tube periphery becomes exceedingly large; in other words, the significant degree of total temperature separation in the radial direction should occur if and when a periodic disturbance with a wave number as $m = 1$ is present. Thus, the confirmation of the vortex whistle to be $m = 1$ type when the Ranque-Hilsch effect exists is crucially important in suggesting a strong likelihood that the vortex whistle is indeed a mechanism for the temperature separation. The wave number of the second, third and fourth harmonics are also identified in a similar manner, to be equal to 2, 3 and 4 respectively. Such existence of the higher harmonics in the expected above form provides further additional support to the argument that the temperature separation is caused by acoustic streaming.

Once, m is found to be 1, circulation Γ and the radius of the tube r_o are given, the comparison of the measured f with the calculated values based on the linearized theory can be made. In terms of the frequency, f, Eq. (4.5) becomes

$$f = \frac{\omega}{2\pi} = \frac{1}{2\pi} \frac{\Gamma}{r_o^2}$$

Γ may be estimated from the Kelvin's theorem by assuming that its value around the tube periphery is equal to the one around the circumference at the exit of the swirl generator. The tangential velocity is estimated, given the injection angle and injection nozzle area, from the

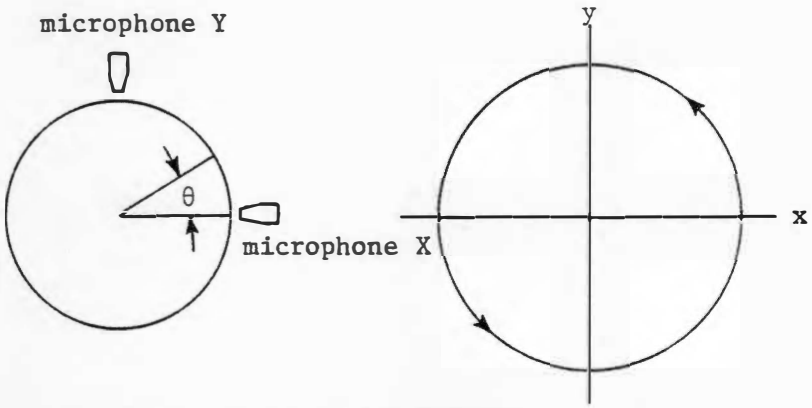

a. Trajectory of signals received by two microphones 90° apart

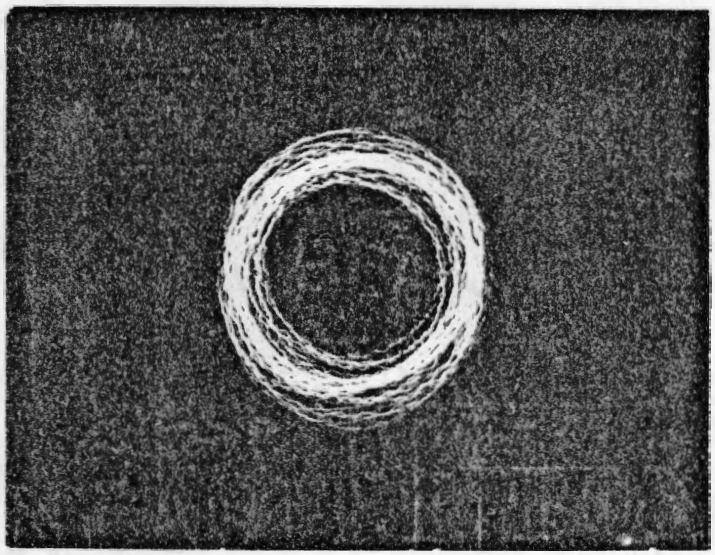

b. Lissajous figure for 90° microphone arrangement

Figure 8. Tangential wave number trajectory for 90° microphone arrangement.

volume flow rate determined from the mass flow measurement and static pressure tap installed on the cold end plug. For a 1.65 inch solid tube, it is readily observed that the measured frequency is in reasonable agreement with the theory. The discrepancy may be considered to be due to the slow-down of swirl through the tube of 1.65 inches. Thus a shorter tube of 0.5 inches in length is tested. For a 0.5 inch tube, the results shown in Figure 9 indicate an excellent agreement. Although the spiky peaks for the shorter tube are not as distinct as that for 1.65 inch tube, they are still well defined. Figure 10 typifies the frequency spectra for this shorter solid tube.

b. Porous Vortex Tube With Acoustic Suppressors

Upon the completion of the tests described above, the main pipe of smooth brass is replaced with a porous pipe of the same length and diameter, where a number of holes of 0.046 inches in diameter are drilled. In its initial arrangement, the holes form a staggered array, 45 rows in the circumferential and 25 in the axial direction. Upon this porous pipe, one fits a larger Teflon section, where acoustic cavities of 0.173 inches in diameter, 8 in the axial and 12 in the circumferential, are drilled; those holes on the tube that do not match with the acoustic cavities are identified and refilled with plastic filler in order to remove any unnecessary irregularity on the inner surface of the pipe. By this, on the average a group of six holes upon the brass section match with each acoustic cavity and porosity turns out to be around 27%. By inserting plexiglas tuning rods into each cavity and adjusting its length, ℓ, variable from 0.9 inches to zero, the vortex whistle at any desired frequency can be Teflon section is covered by a sheath of solid Teflon and furthermore, is fastened by clamps. The entire test rig assembly is shown in Figure 11.

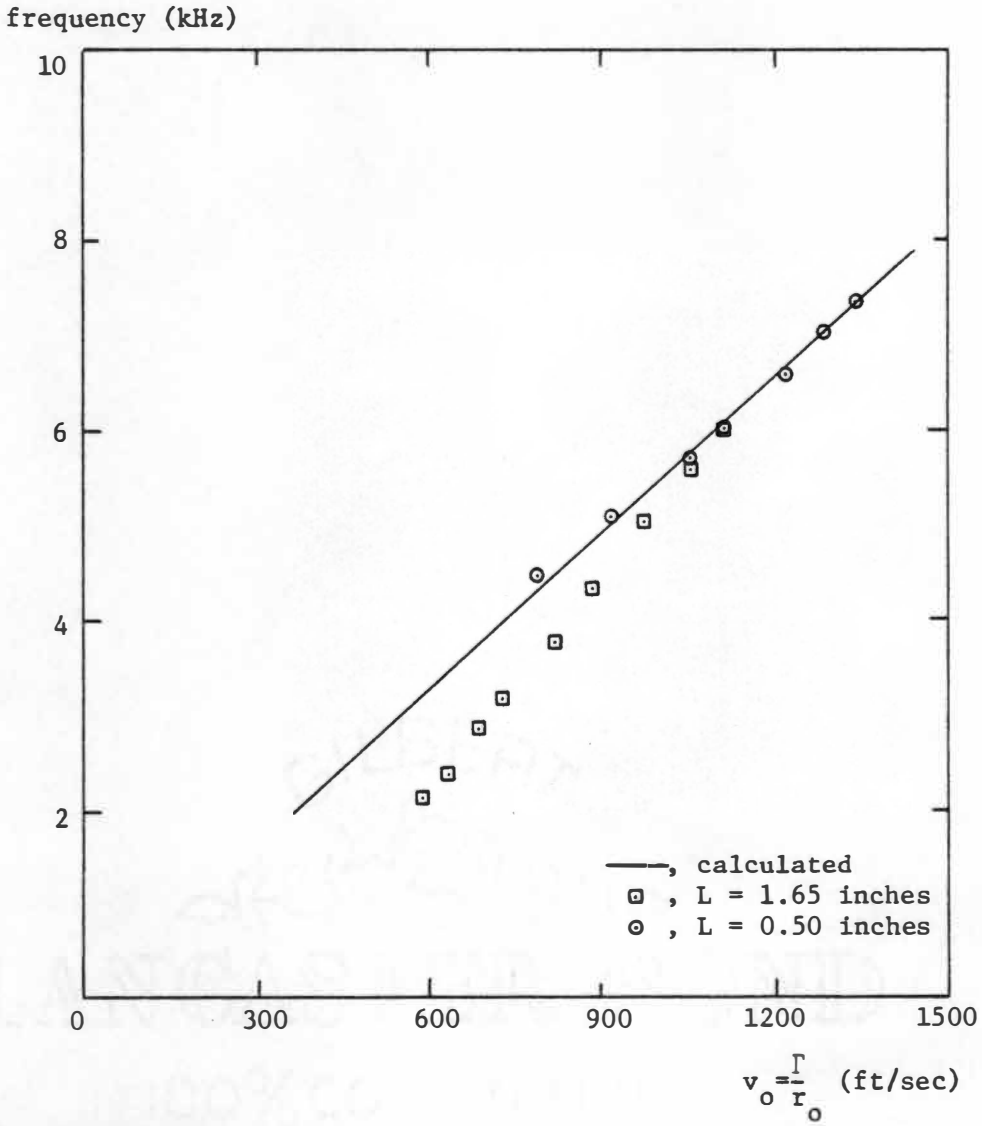

Figure 9. Fundamental frequency for solid pipe.

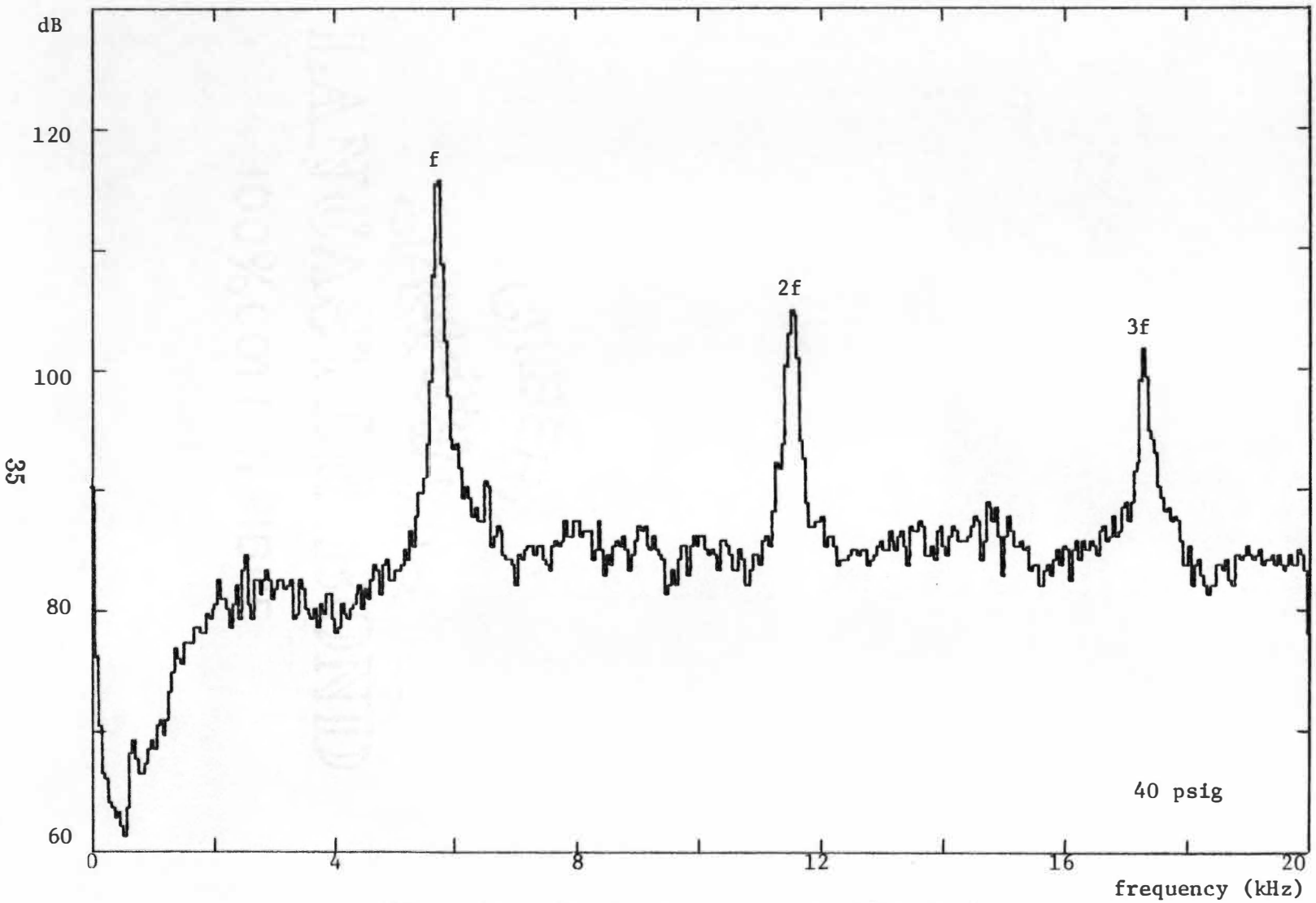

Figure 10. Frequency spectrum for 0.5 inch pipe.

To make sure that the modification of the main tube from a smooth wall to a porous one does not significantly alter the temperature separation and the basic characteristics of the vortex whistle, initially all tuning rods are pushed in so that all cavity lengths become zero. In the next section, this will be described, followed by the discussion on the results of a non-zero cavity length.

1. Zero Acoustic Cavity Length

The results are shown in Figure 12. Only the measured frequency is noticeably affected, lowered by 15% from smooth tube as might be expected from the slowdown of swirl due to the presence of porous wall. Except for this, the temperature separation (Figure 12a) and frequency spectra remain virtually the same as the solid wall; the wave numbers are unchanged and the vortex whistle retains its spiky peaks. Thus the change to a porous tube did not inadvertently alter the characteristic of the solid tube.

2. The Effect of Suppression of Vortex Whistle Upon Temperature Separation

aa. Thermocouple at position a of Figure 11

Figures 13 through 18 show, in sequence, the effect of suppressing the vortex whistle upon the temperature separation. Each figure consists of a set of three data: ΔT^*, sound level and frequency. The length of the acoustic cavities is as follows: $\ell = 0.9, 0.8, 0.7, 0.6, 0.5$ and 0.4 inches and the thermocouple at the centerline is left at the cold spot, which corresponds to the position a of Figure 11. In each case, the length of all acoustic cavities is uniformly equal. As obvious from these Figures, as the inlet pressure goes up slowly, the temperature separation keeps on increasing, as in the case

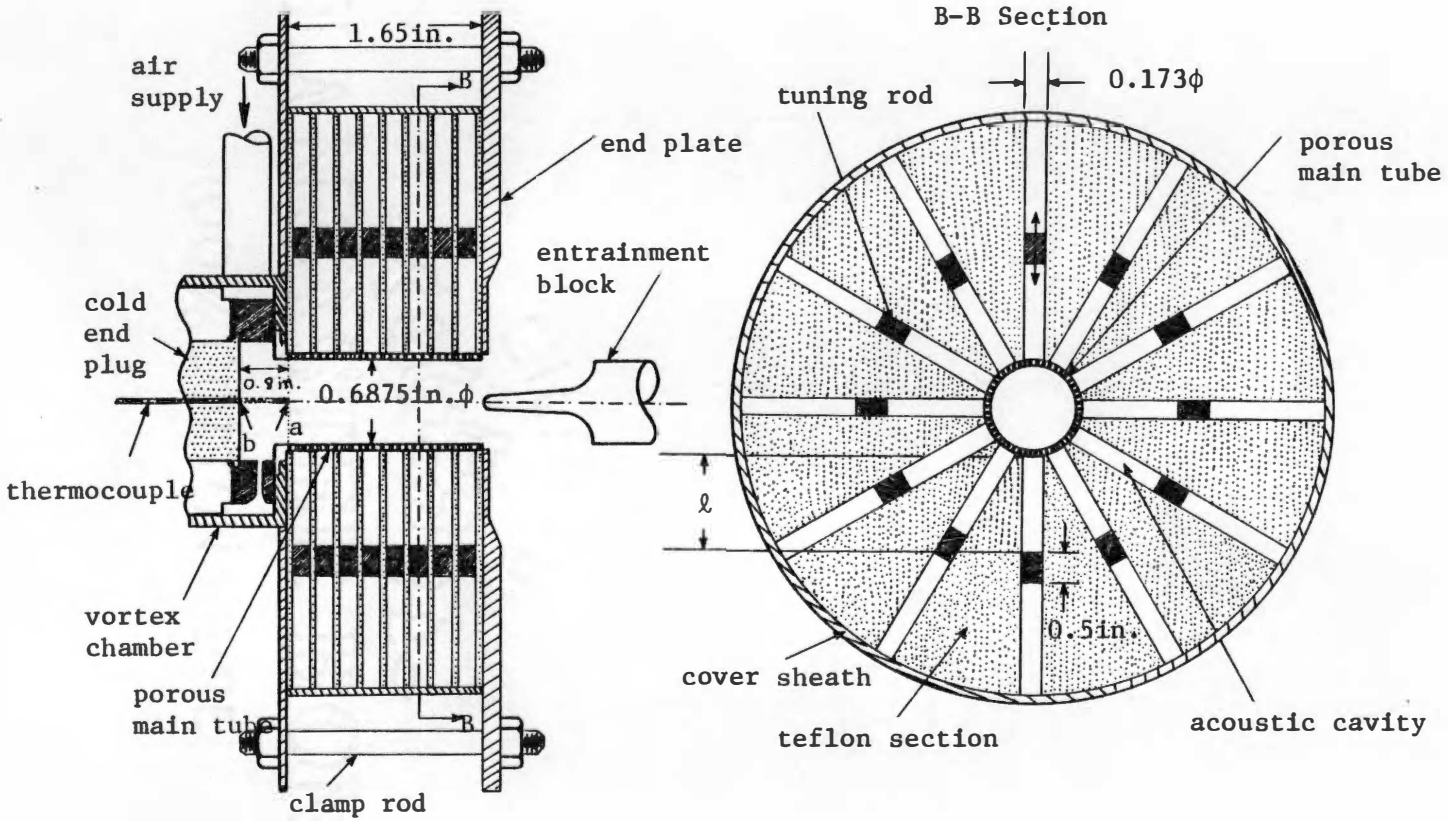

Figure 11. Layout of test rig: porous main tube with acoustic suppressors.

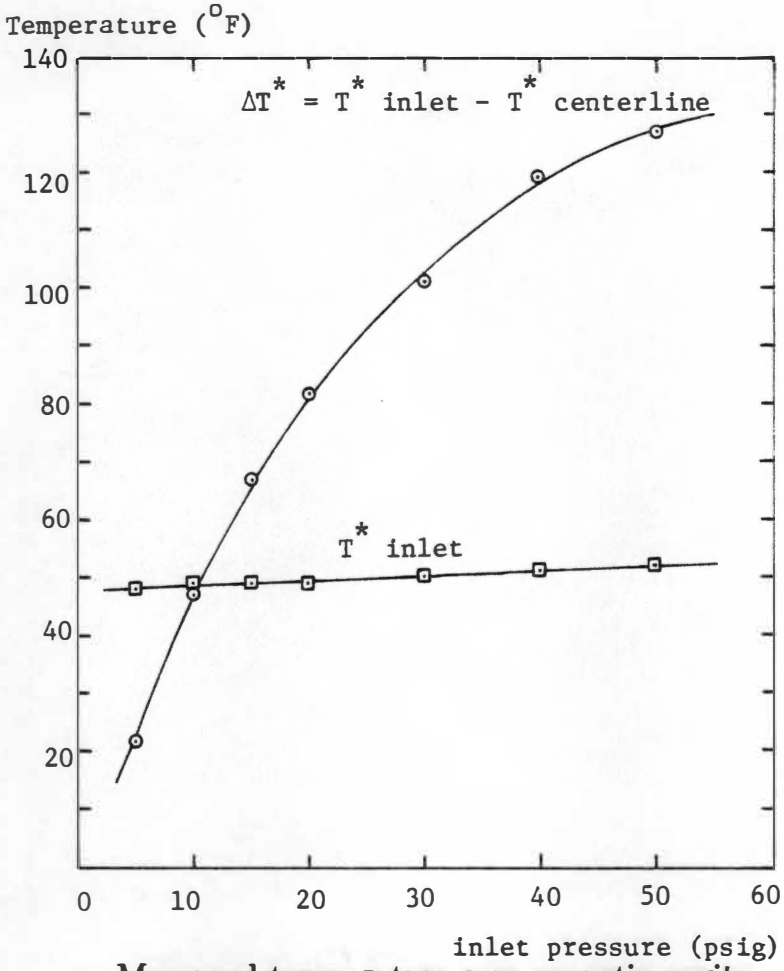

a. Measured temperature zero acoustic cavity

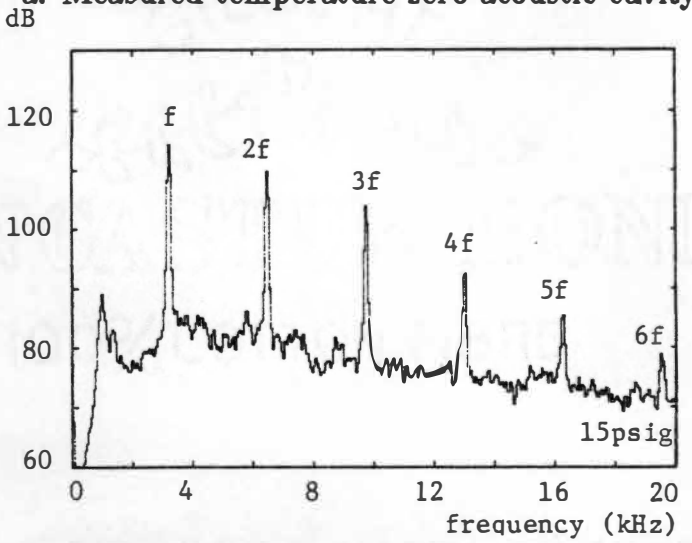

b. Frequency spectrum for zero acoustic cavity

Figure 12. Data for zero acoustic cavity at cold spot position.

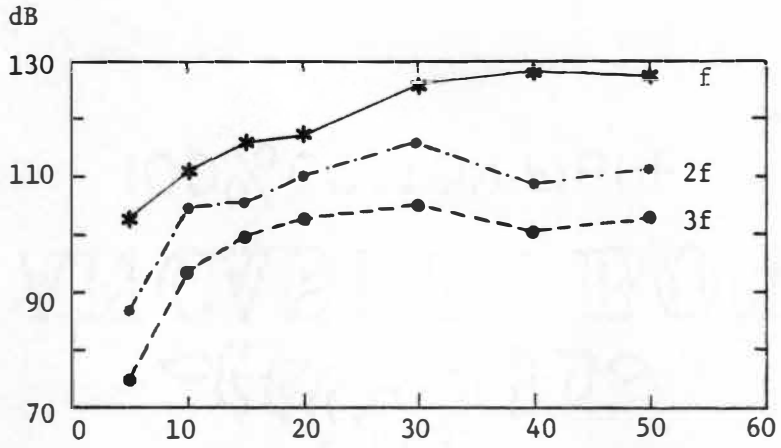

c. Sound level for zero acoustic cavity

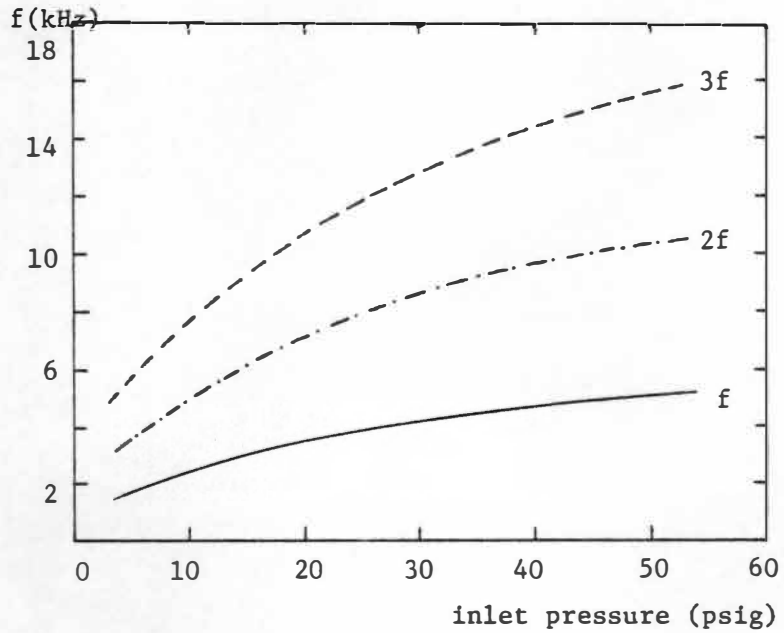

d. Frequency for zero acoustic cavity

Figure 12. (continued)

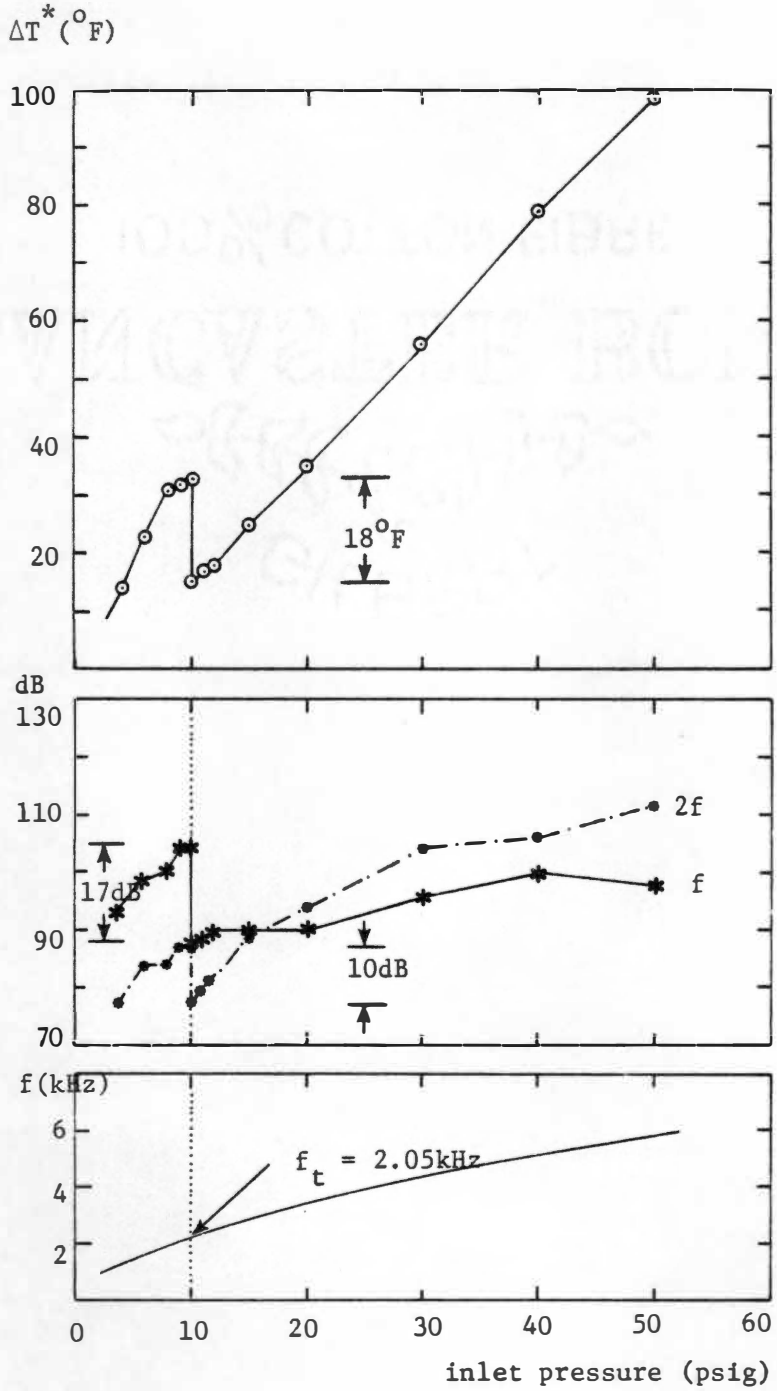

Figure 13. Data for 0.9 inch acoustic cavity length at cold spot position.

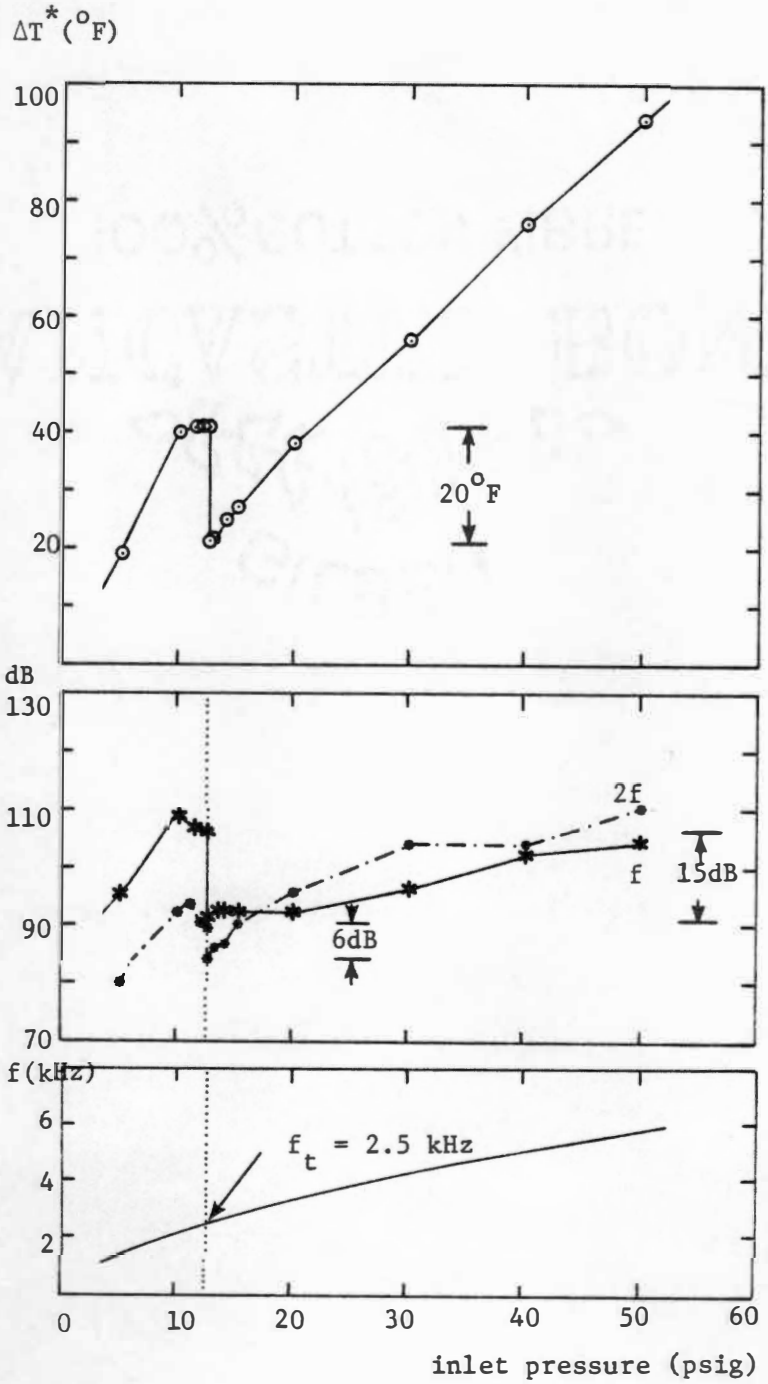

Figure 14. Data for 0.8 inch acoustic cavity length at cold spot position.

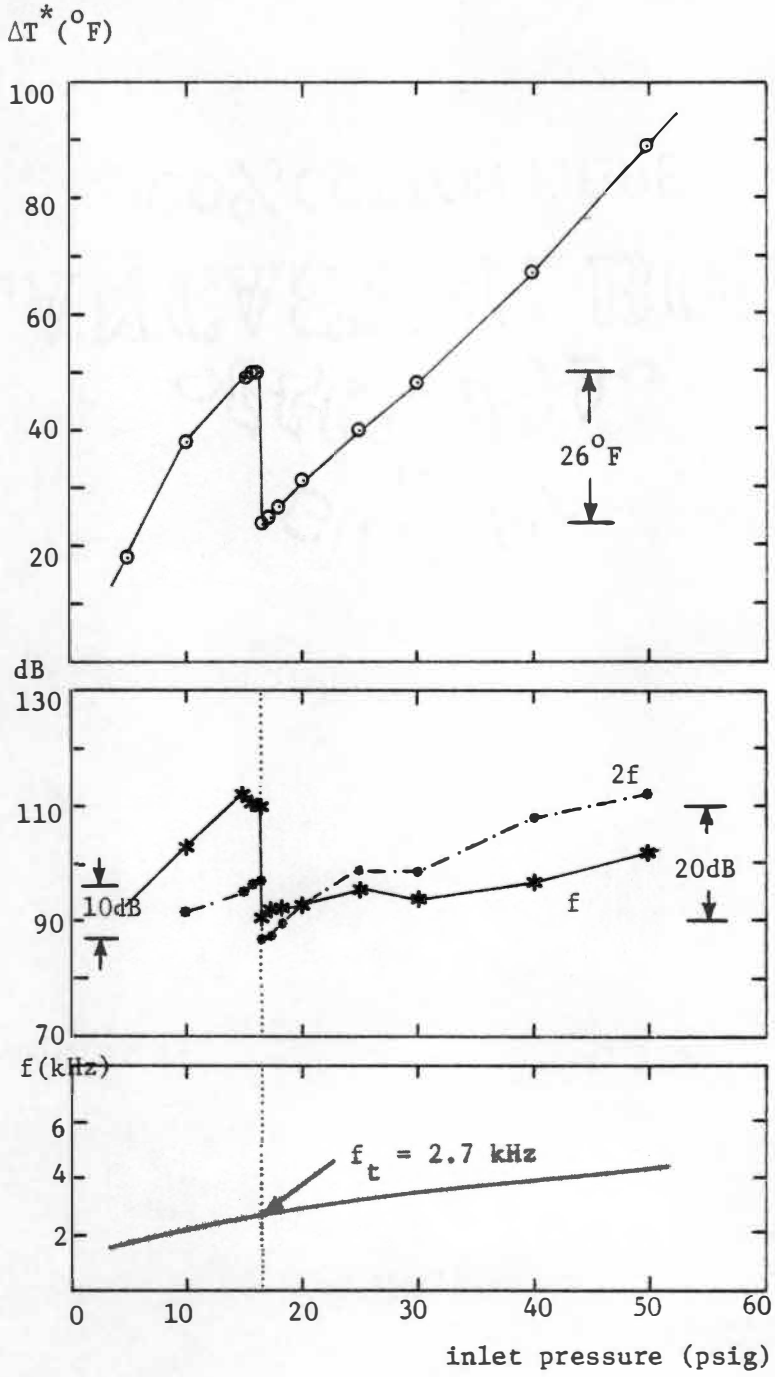

Figure 15. Data for 0.7 inch acoustic cavity length at cold spot position.

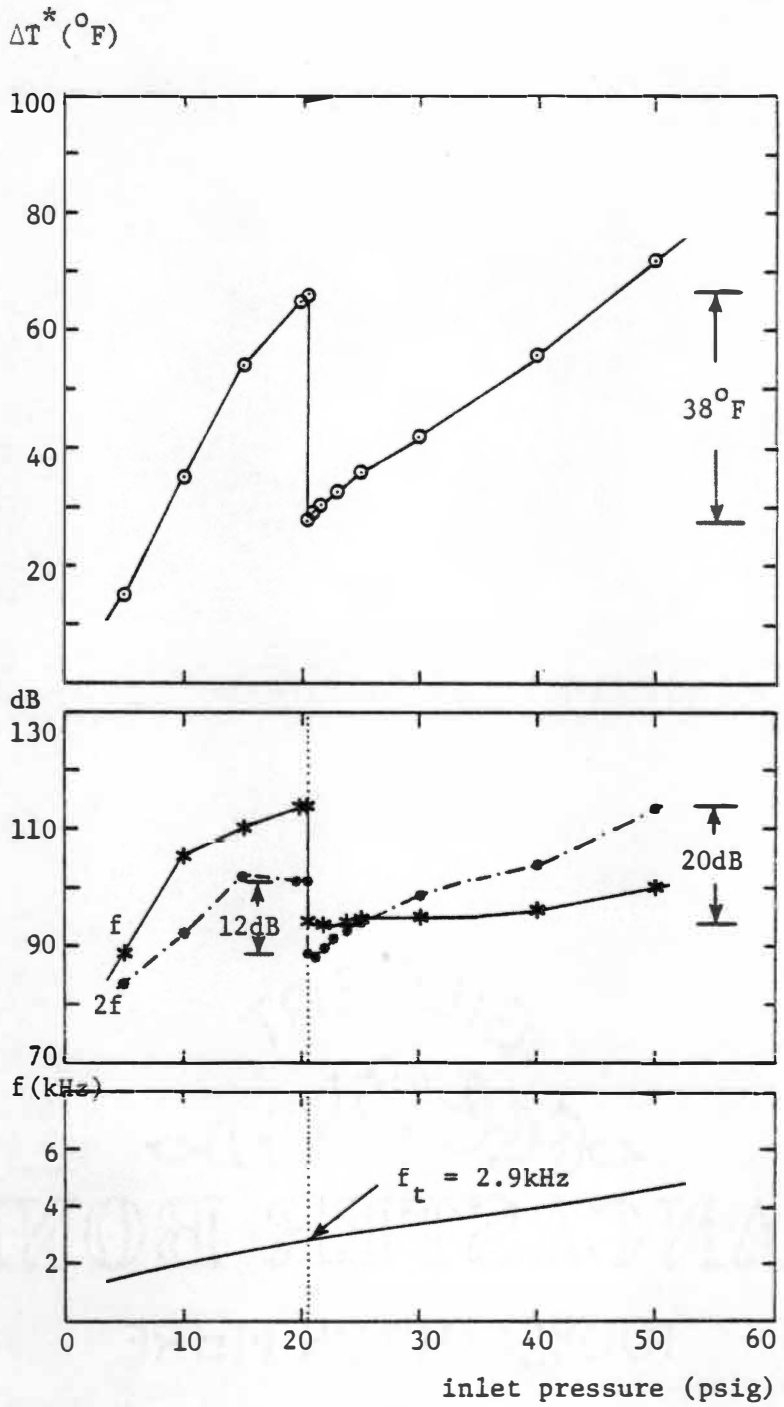

Figure 16. Data for 0.6 inch acoustic cavity length at cold spot position.

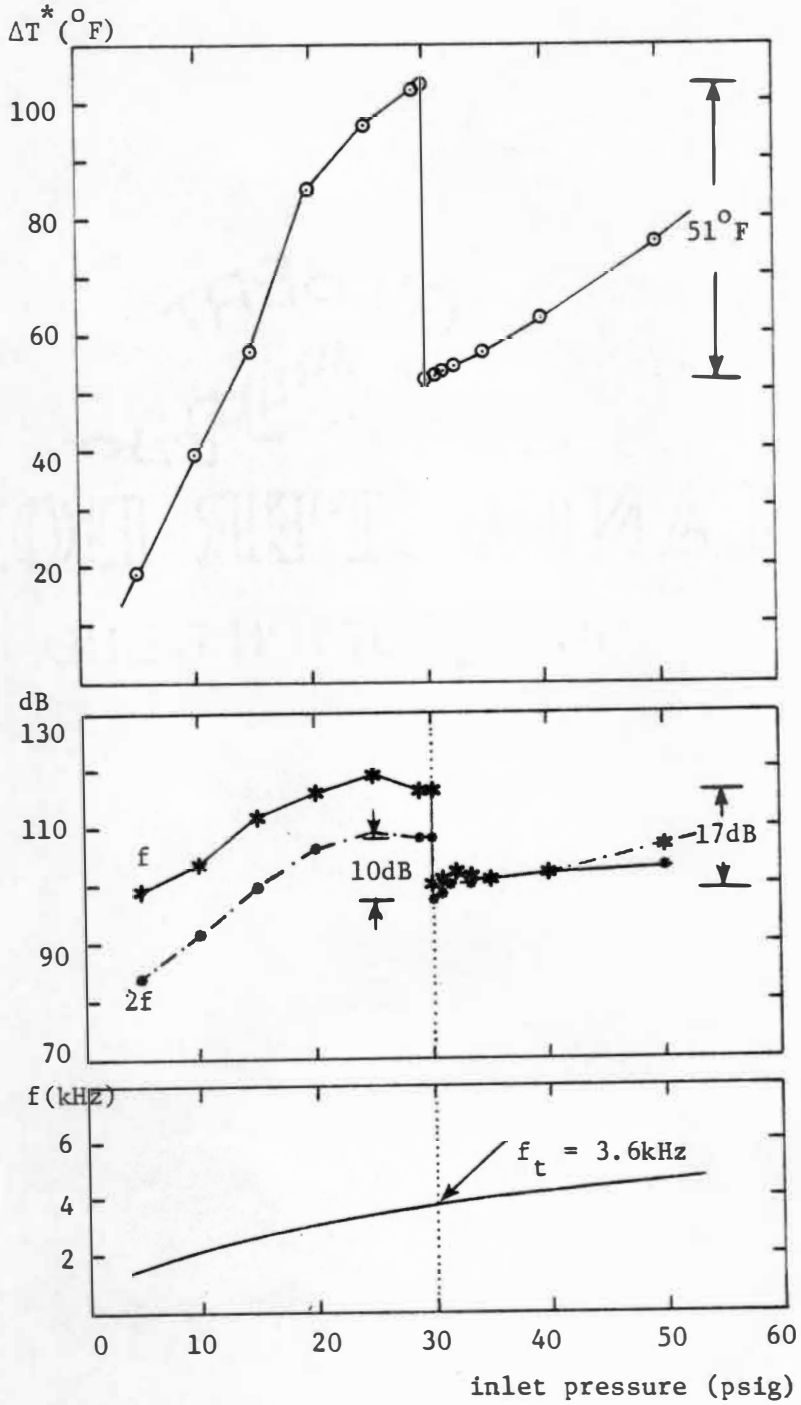

Figure 17. Data for 0.5 inch acoustic cavity length at cold spot position.

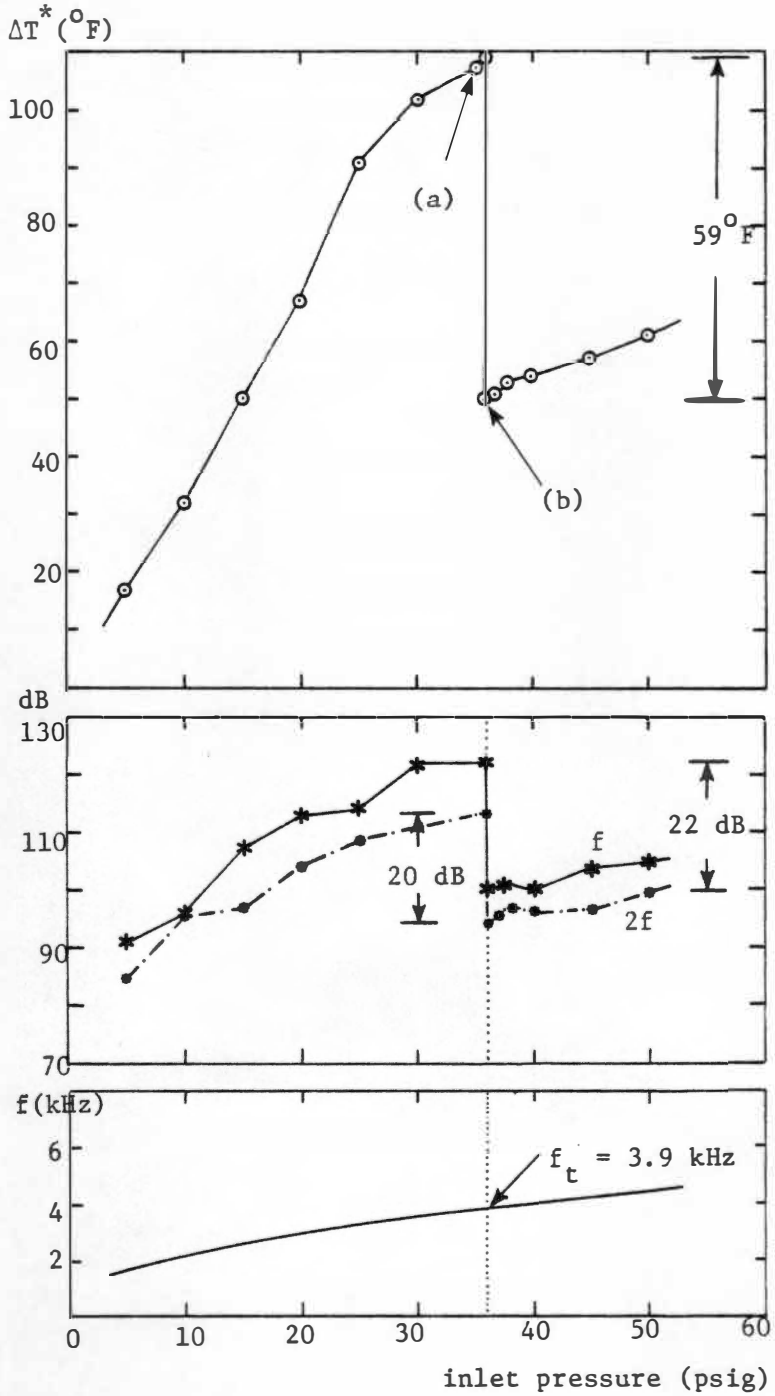

Figure 18. Data for 0.4 inch acoustic cavity length at cold spot position.

of zero cavity – until at the very instant when f hits any tuned frequency, f_t, all of a sudden the sound levels take a sudden plunge, changing from a shrill whistle to a muffled hiss; at that moment, the centerline temperature immediately leaps upward, leading to a sudden fall in ΔT^*; for example, for $\ell = 0.5$ inches corresponding to the tuned frequency $f_t = 3.6kHz$, the sound level of the fundamental frequency plummets down by $17dB$ and the second harmonic by $10dB$; at that point the centerline temperature, which has gone down to -48^oF, instantaneously jumps up to $+3^oF$, with a corresponding sudden loss of temperature separation equal to 51^oF.

The successive change of the sound level at the tuned condition can be observed from the frequency spectra. Figure 19 illustrates this for the acoustic cavity length $\ell = 0.4$ inches; in (a), which corresponds to the inlet pressure of 35psig, a point slightly below the tuned condition indicated in Figure 18, the spiky peaks are distinct and dominant; in (b), which now corresponds to the inlet pressure of 36psig, the tuned condition in Figure 18, the substantial portions of peaks are diminished. At the same time, the bases of the vortex whistle, as measured by the externally placed microphone, appear to become broadened ('haystacking') and lose their distinctive characteristics of dominant peaks. As discussed earlier, at this condition the temperature separation reduces more than half of its value at (a). As the frequency is increased further, the vortex whistle starts to recover its spires, at the same time the cold temperature at the centerline begins to fall again.

Note that the reduction of the sound level of the fundamental harmonic, to whose frequency the cavity length is tuned, does cause the reduction in the second harmonic as well; this appears to reveal that the second

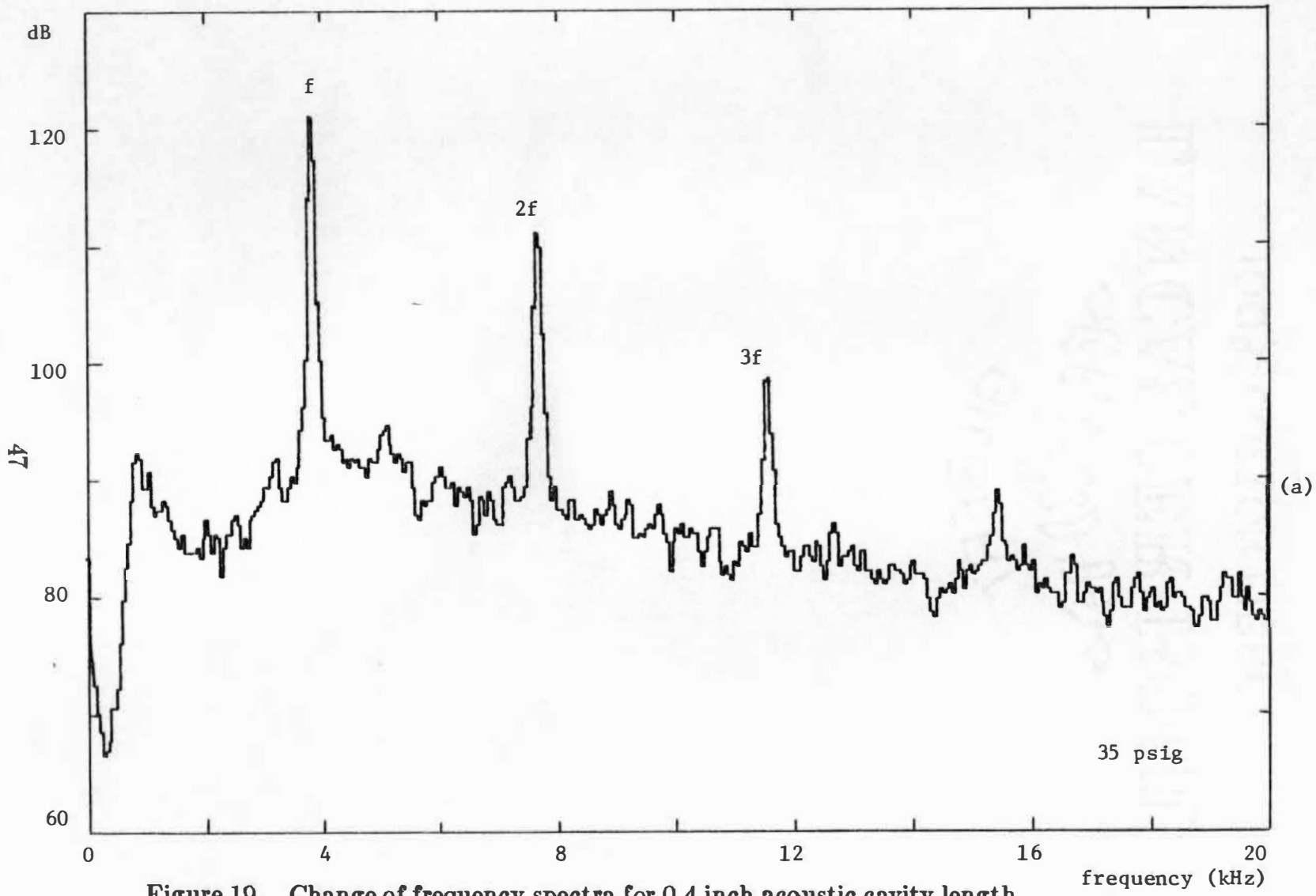

Figure 19. Change of frequency spectra for 0.4 inch acoustic cavity length.

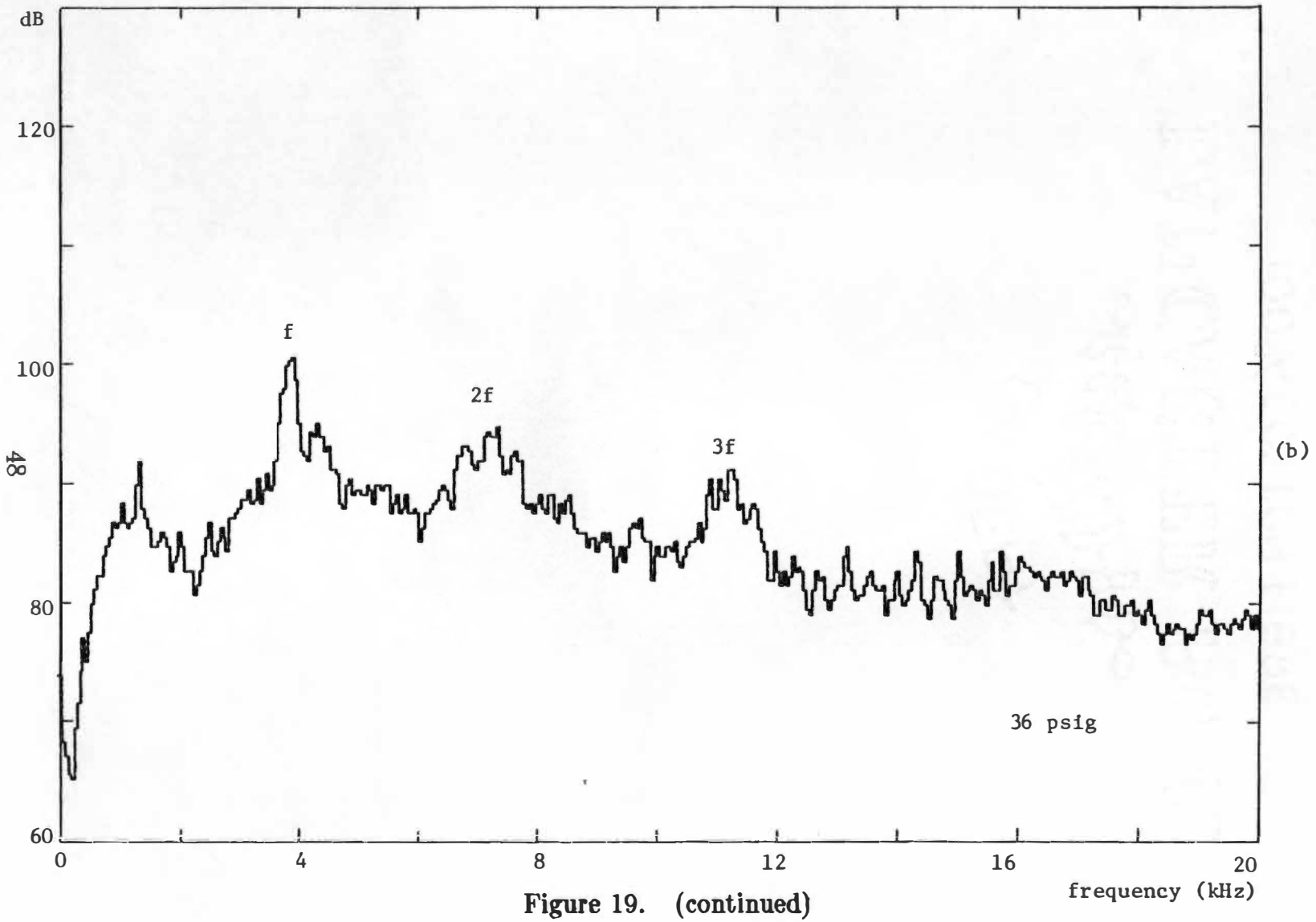

Figure 19. (continued)

harmonic is induced by the fundamental one. Since the attenuation of the pure tone at f_t did not completely suppress the vortex whistle, it seems possible that by suppressing the sound level some more, the temperature separation could be reduced further.

In light of this – and although the temperature separation in the Ranque-Hilsch tube is not wholly attributable to acoustic streaming induced by the vortex whistle since the innermost core of any Rankine vortex must have total temperature gradient caused by viscous stresses perhaps of the order of 10^oF – it appears clear that acoustic streaming induced by the orderly periodic disturbances is the dominant mechanism of the Ranque-Hilsch effect.

bb. Thermocouple at position b of Figure 11

As indicated, the data shown in Figures 13 through 18 were taken with the thermocouple at the centerline placed at the cold spot. To confirm that the intrusion of the thermocouple does not inadvertently trigger the aforementioned sudden change, the thermocouple is withdrawn and placed flush with the Teflon plug (position b of Figure 11). Then there is nothing in the way of the flow path. The basic features in Figure 20 for zero acoustic cavity and Figures 21 through 26 are the same as before: at the same f_t the sound level falls precipitously and this is accompanied by a loss of temperature separation. The only essential difference is the lesser amount of ΔT^* drop, which corresponds to the higher level in ΔT^* at position a.

A striking transformation in flow takes place all at once at the tuned condition. This, though not adequately recorded, can easily be felt with a touch of the hand at the exhaust. Below the tuned condition, the flow is swirling swiftly near the tube periphery and outside of it, over the

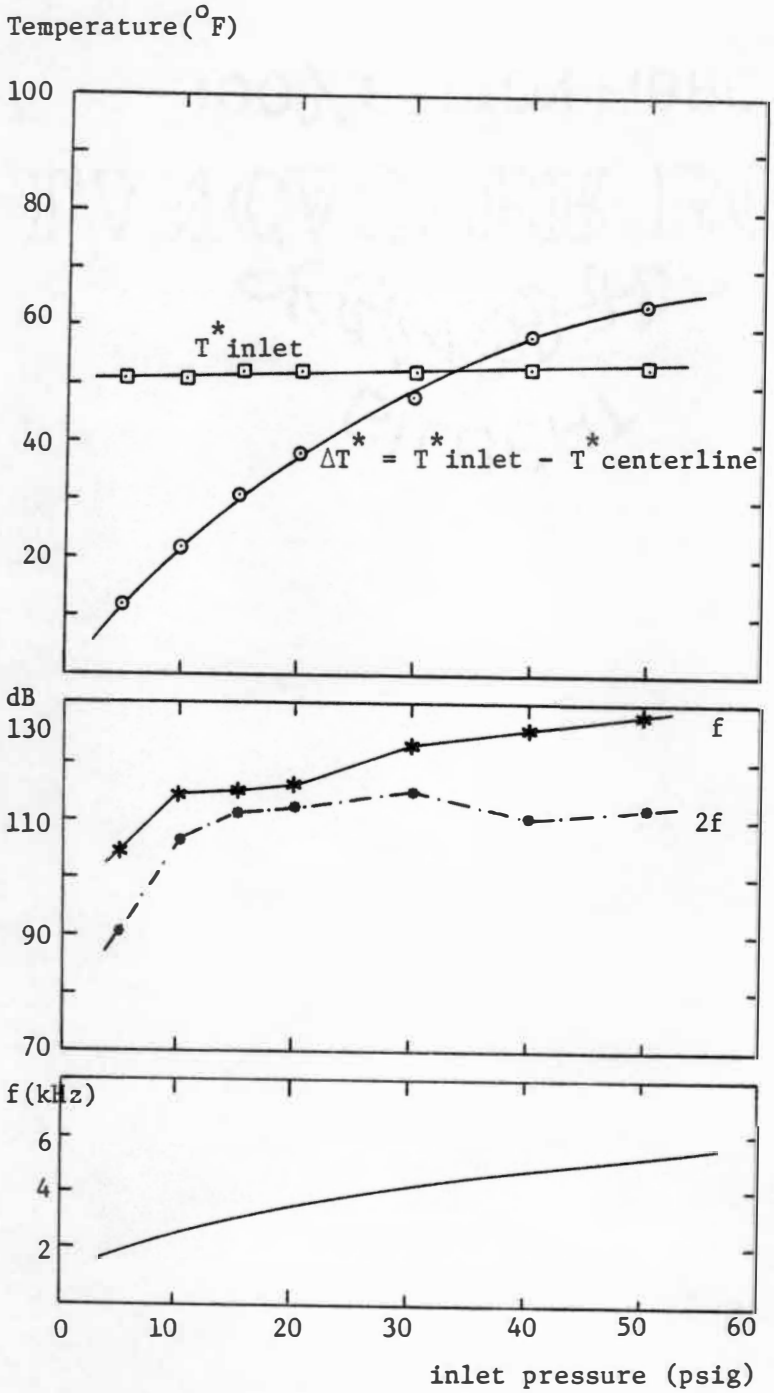

Figure 20. Data for zero acoustic cavity at flush position.

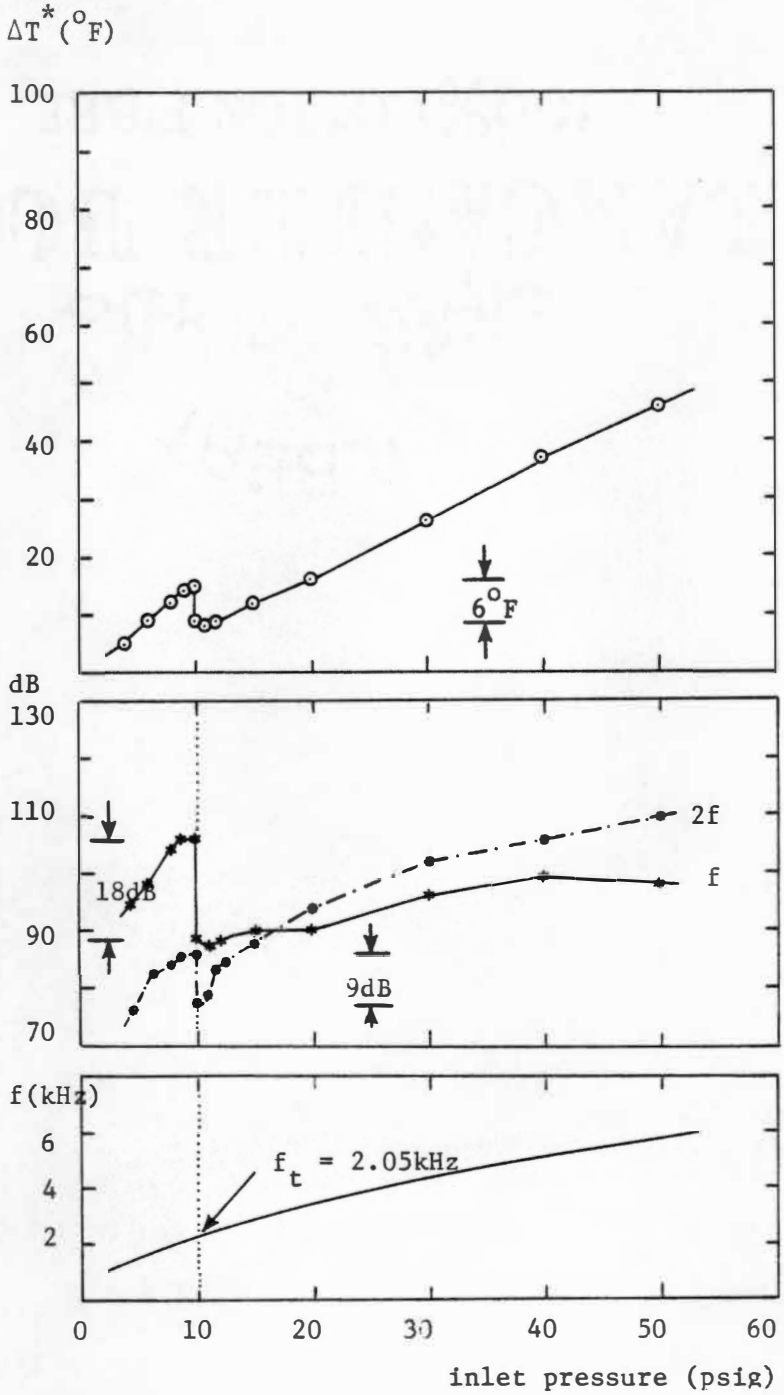

Figure 21. Data for 0.9 inch acoustic cavity length at flush position.

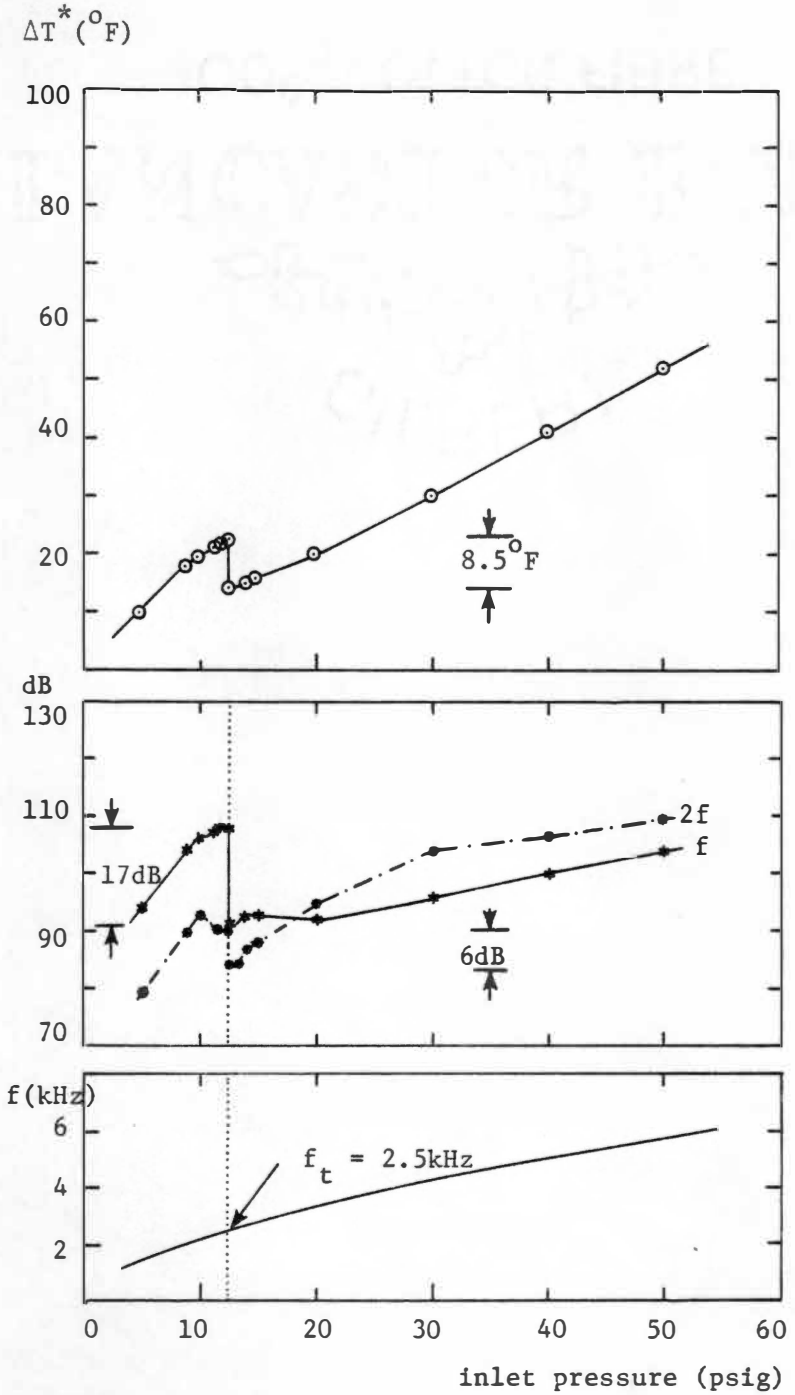

Figure 22. Data for 0.8 inch acoustic cavity length at flush position.

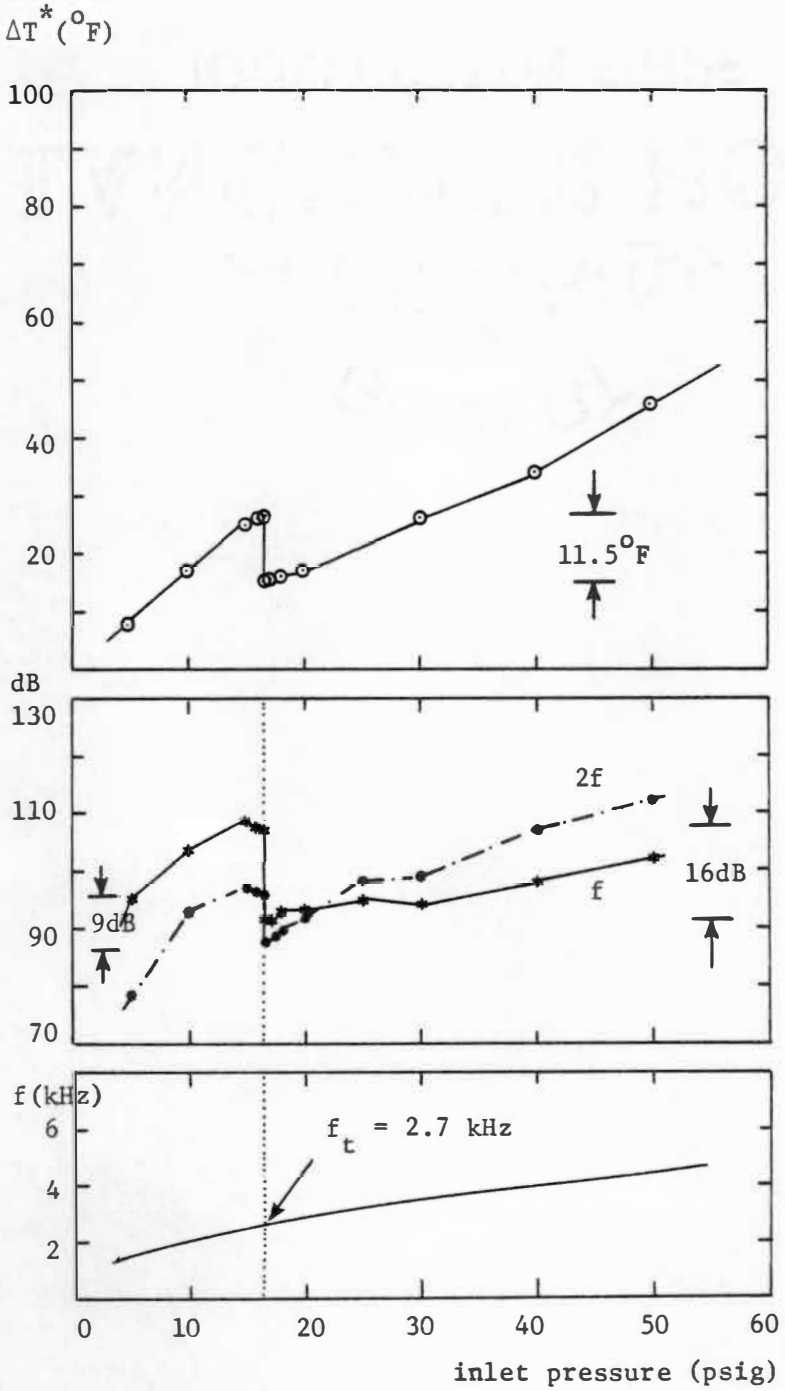

Figure 23. Data for 0.7 inch acoustic cavity length at flush position.

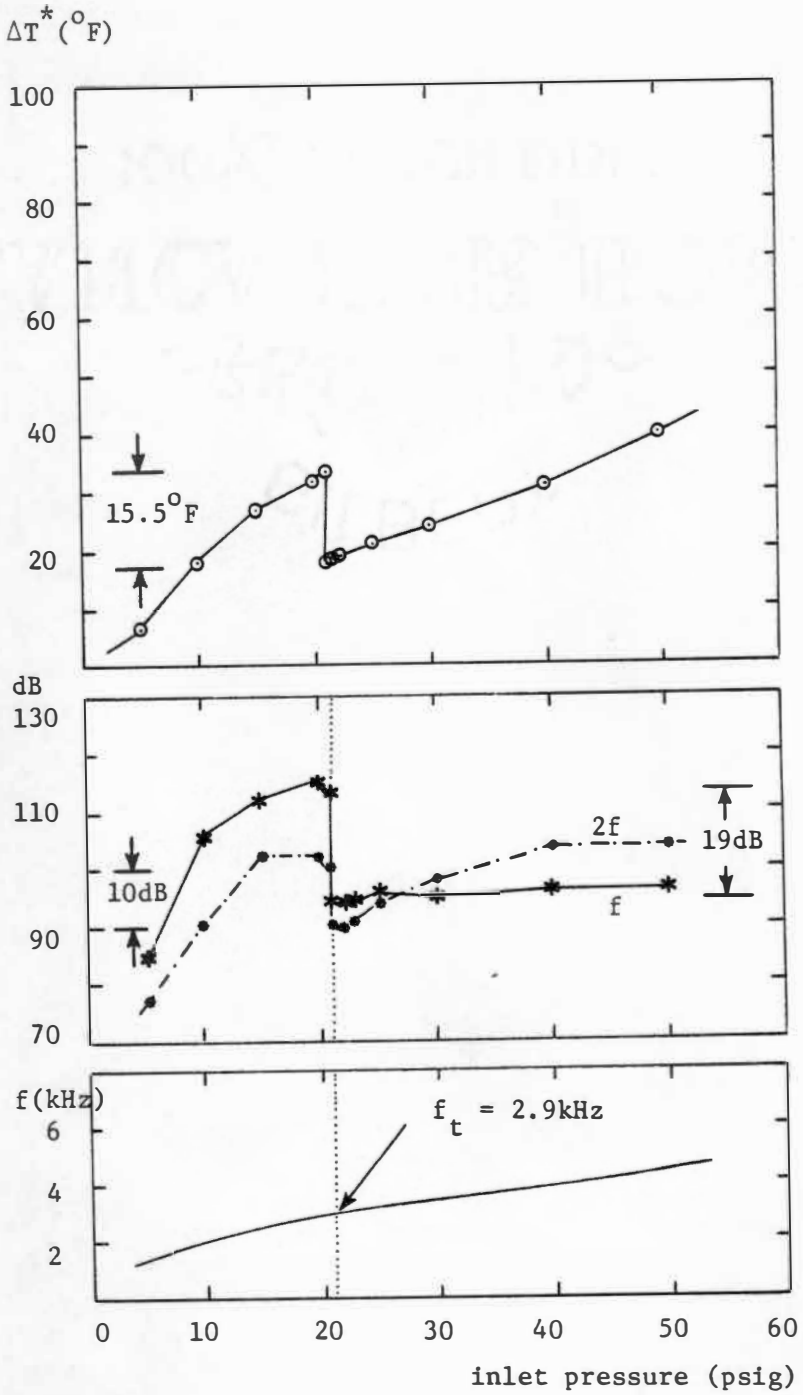

Figure 24. Data for 0.6 inch acoustic cavity length at flush position.

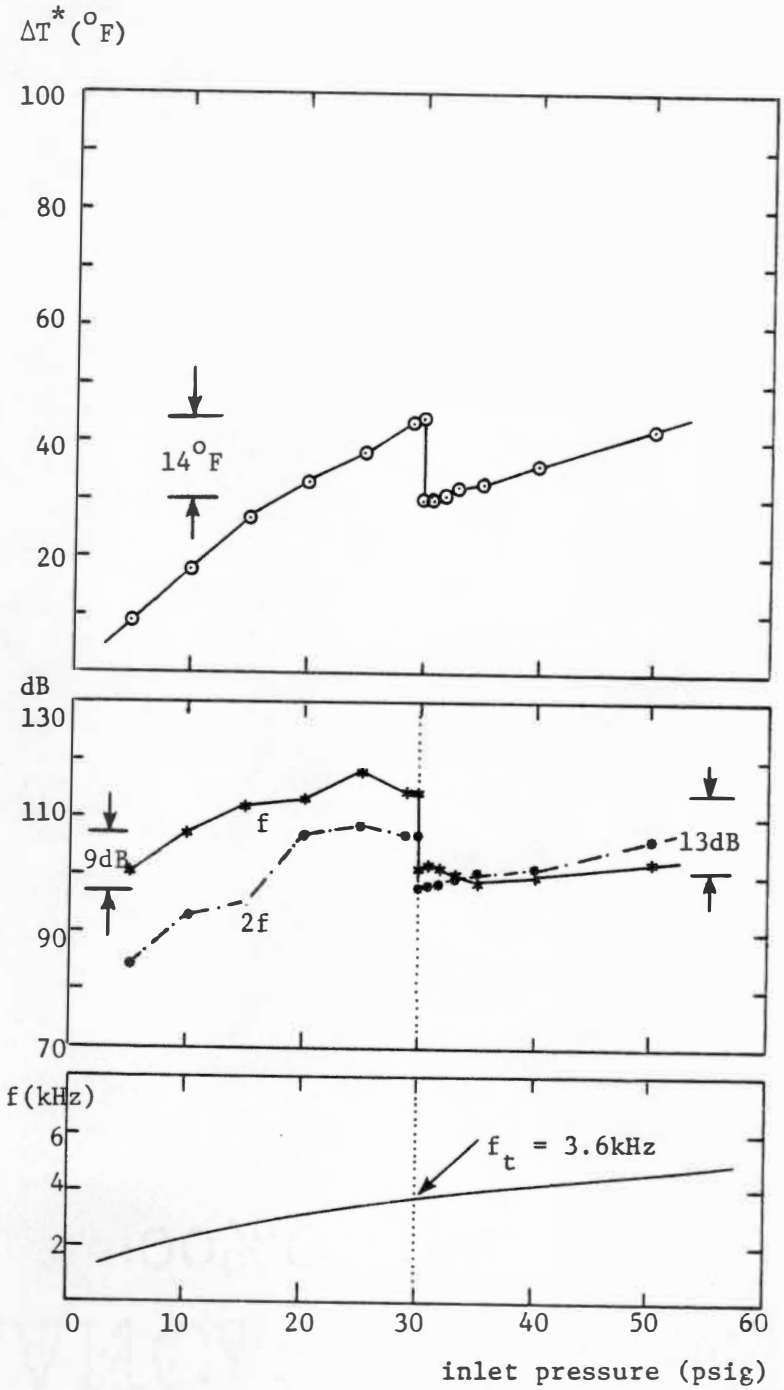

Figure 25 Data for 0.5 inch acoustic cavity length at flush position.

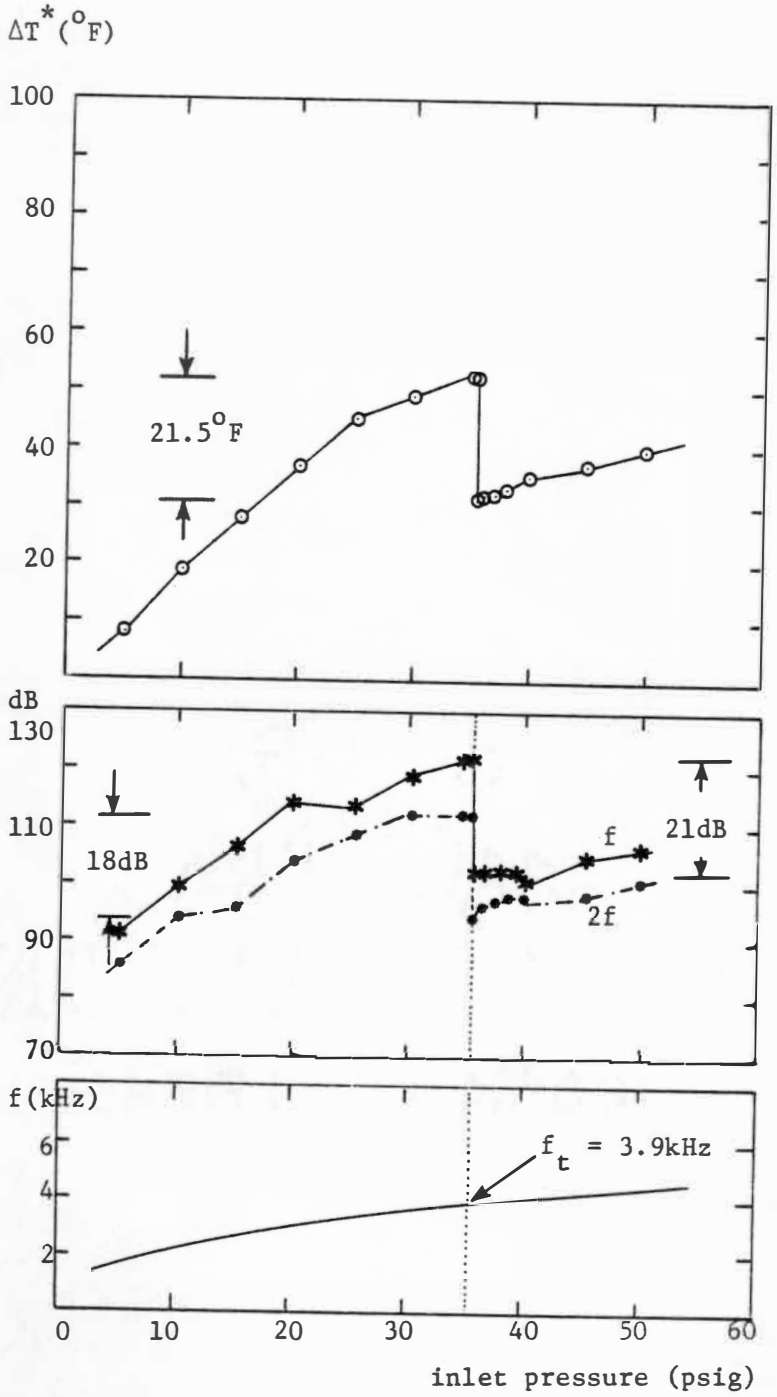

Figure 26. Data for 0.4 inch acoustic cavity length at flush position.

surface of the end plate (a sketch in Figure 27a); on the other hand, the center core is calm – reminiscent of the eye of a hurricane. At the tuned condition, however, the region near and outside the tube periphery becomes immediately quieter; the swirling air suddenly rushes out along the tube centerline (Figure 27b). This transformation appears to give evidence of the reversion from a forced vortex (below the tuned condition) to a Rankine vortex (at the tuned condition) – the expected reversion of the very process induced by acoustic streaming and depicted previously in Figure 3 (Page 21).

c. Upscale Version of the Ranque-Hilsch Tube

The size of the test rig, used for all the aforementioned tests with the tube of 0.6875 inches in diameter, is obviously too small for the radial traverse of total temperature. The initial attempts for such a traverse have to be aborted since the radial immersion of a probe into the flow is itself found to cause severe interference with the measurement; a similar difficulty was also reported by Reynolds [10]. Therefore, an upscale version of the test rig is built to facilitate the radial traverse. The diameter of the main tube is now 2 inches. Compared to the smaller version, this and other major dimensions are enlarged with a scaling factor of 3; only the size of porous holes on the main tube and the diameter of the acoustic cavities remain the same as the smaller rig. The swirl is again created by a swirl generator, a stationary ring with four tangentially drilled slots. Figure 28 shows the layout of the upscale version of the uniflow type Ranque-Hilsch tube. The tests performed in the upscale rig reconfirmed the conclusions reached by the small rig. In addition, the enlarged size now enables one to insert probes radially and carry out traverses.

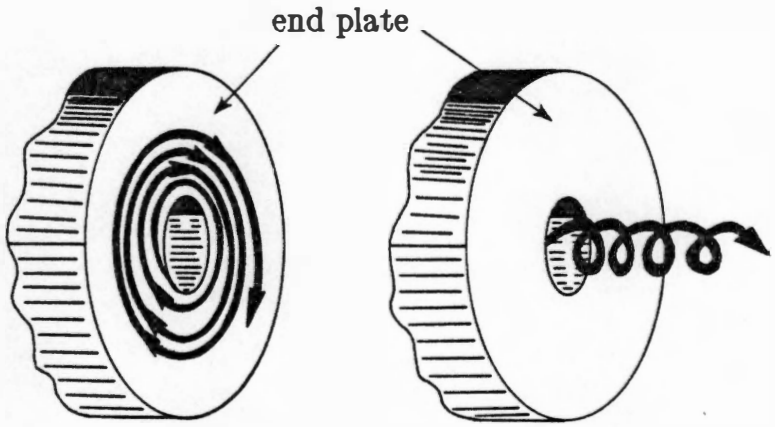

(a) before tuned frequency (b) at the tuned frequency

Figure 27. Transformation of flow pattern at the tuned condition.

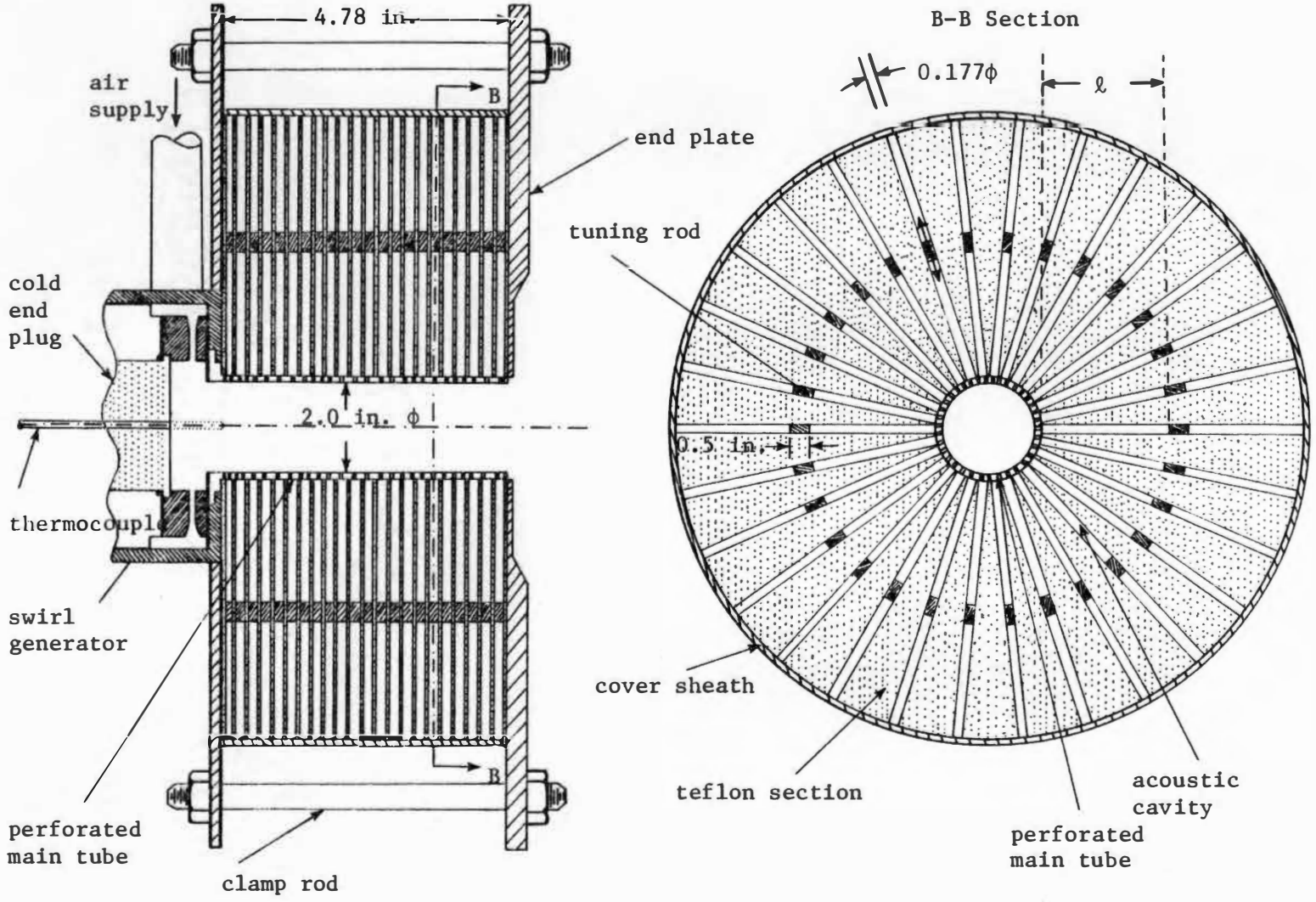

Figure 28. Layout of upscale version.

Even though the tube is now enlarged in diameter, the introduction of such radial temperature probes into the vortex flow still produces interference in the fields within the tube. For example, consider the interference between the following two thermocouples: (1) the centerline thermocouple inserted through the cold end plug to monitor the temperature there, (2) and the other probe, the radial thermocouple, gradually inserted at a position corresponding to the twelfth (12) axial cavity (1.3 inches from the tip of the centerline thermocouple). With the inlet pressure held constant, the radial temperature probe is inserted and approaches the centerline; the temperature as measured by the centerline thermocouple changes by $5^{o}F$. The change will, of course, gradually disappear as the probe is withdrawn from the tube centerline. Despite this interference problem, the data to be presented here are considered to show the correct, qualitative trend.

In the following sections, the baseline results – data for zero acoustic cavity – will be presented; this is followed by the discussion on the results for a non-zero acoustic cavity length.

1. Zero Acoustic Cavity Length

Corresponding to zero acoustic cavity length, Figures 29 and 30 show the radial survey of total temperature at 20 and 40 psig, respectively. It is observed that near the periphery the total temperature exceeds the inlet temperature, as expected from the balance of energy on the ground that the temperature near the centerline is lower than the upstream value. A relatively narrow region near the periphery corresponding to the higher temperature balances with a seemingly wider region near the centerline with lower temperature; this is because near the periphery, the radius and hence the annular area is larger. In addition, the axial velocity is expected

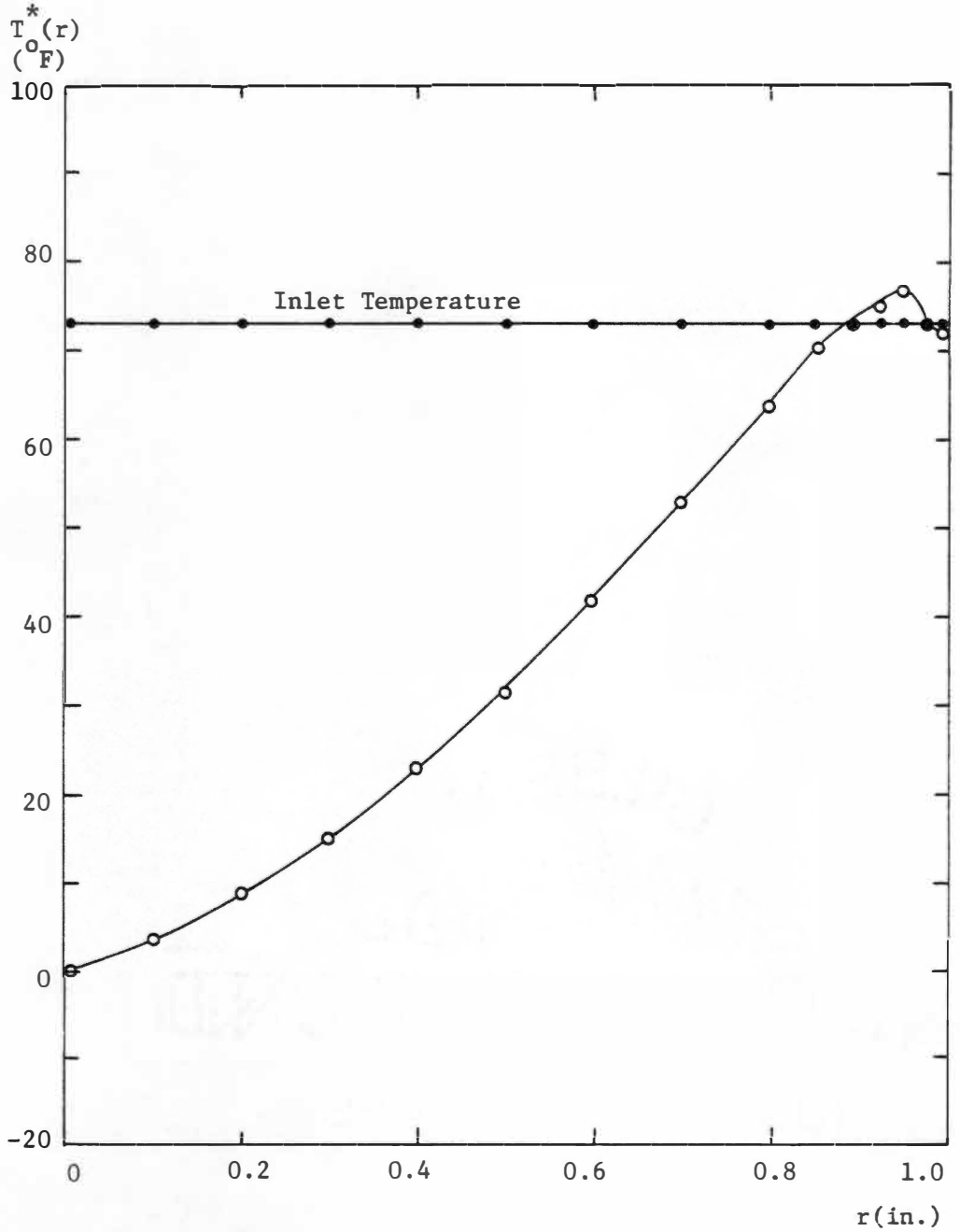

Figure 29. Radial total temperature profile at 20 psig: axial survey position at the fourth (4) acoustic cavity from the manifold end. Zero acoustic cavity length.

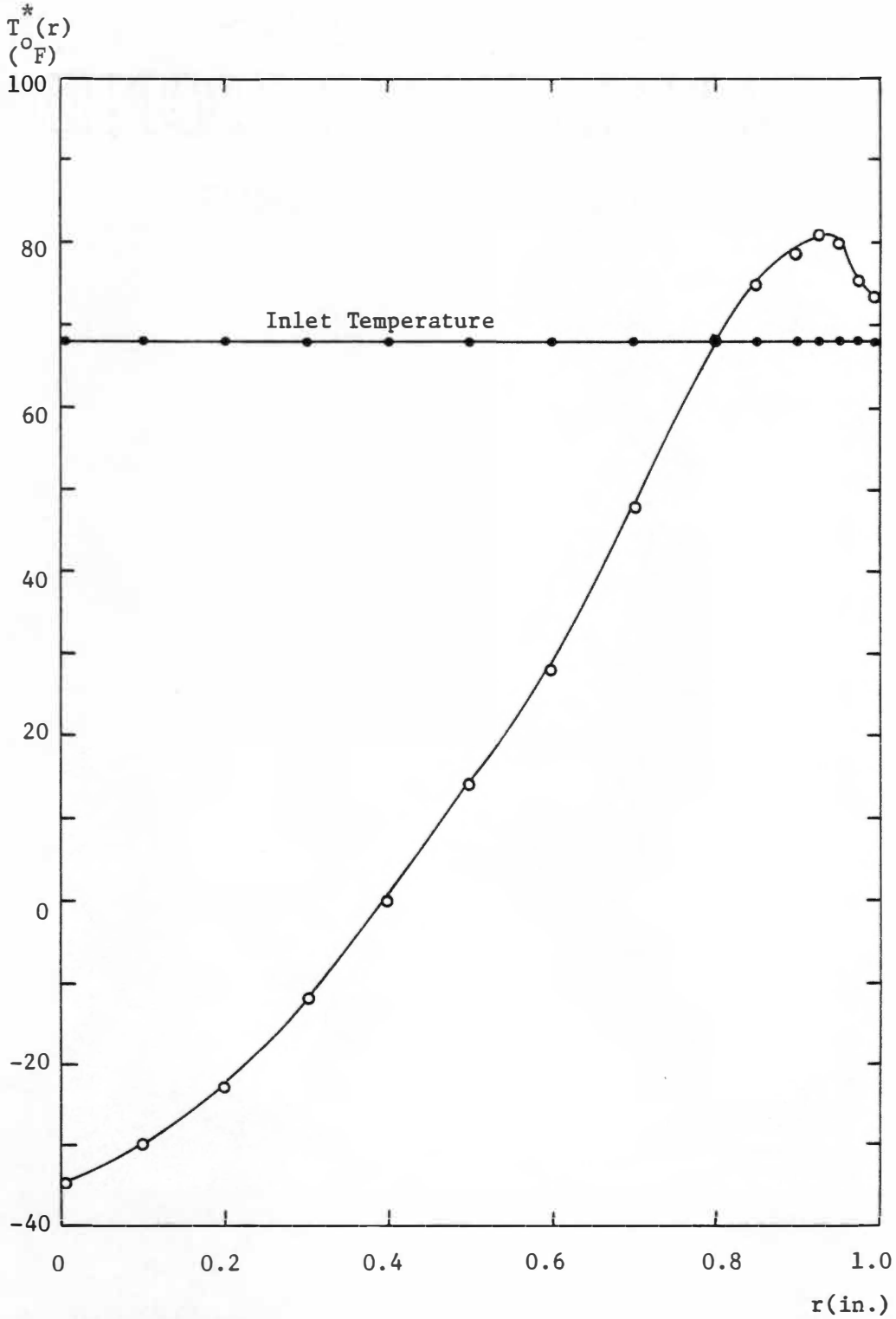

Figure 30. Radial total temperature profile at 40 psig: axial survey position at the fourth (4) acoustic cavity from the manifold end. Zero acoustic cavity length.

to be higher near the periphery, as estimated from the results obtained by Eckert and Hartnett [7].

Figure 31 presents, for zero acoustic cavity, the dependence of the cold temperature at the centerline, together with the record of the inlet temperature; the increase of sound level and frequency is also presented in Figure 31. The result of Figure 31 is qualitatively the same as that of the small scale test rig; quantitatively, the only major difference is that the frequency for the upscale version is much lower, as expected.

2. 1.5 inch Acoustic Cavity Length.

Figure 32 shows the results corresponding to 1.5 inch acoustic cavity length. In addition to the previously measured centerline temperature and inlet temperature, the data of total temperature near the tube periphery is also given. At the moment, the fundamental harmonic hits the tuned frequency, f_t, the sound takes a sudden plunge while the total temperature near the centerline leaps upward as in the case of the small test rig – while the temperature near the periphery drops, as expected from a thermal balance.

Figure 33 presents the radial variation of such a temperature jump as a function of radial positions, where

$$(\Delta T^*)\text{jump} = T^*(\text{after acoustic suppression}) - T^*(\text{before acoustic suppression})$$

near the tube periphery (ΔT^*) jump is negative while near the centerline (ΔT^*)jump is positive. Such a change of the size of (ΔT^*)jump, though to be expected, is confirmed only by the use of large scale test rig; it also enables one to obtain the results of Figures 29 and 30.

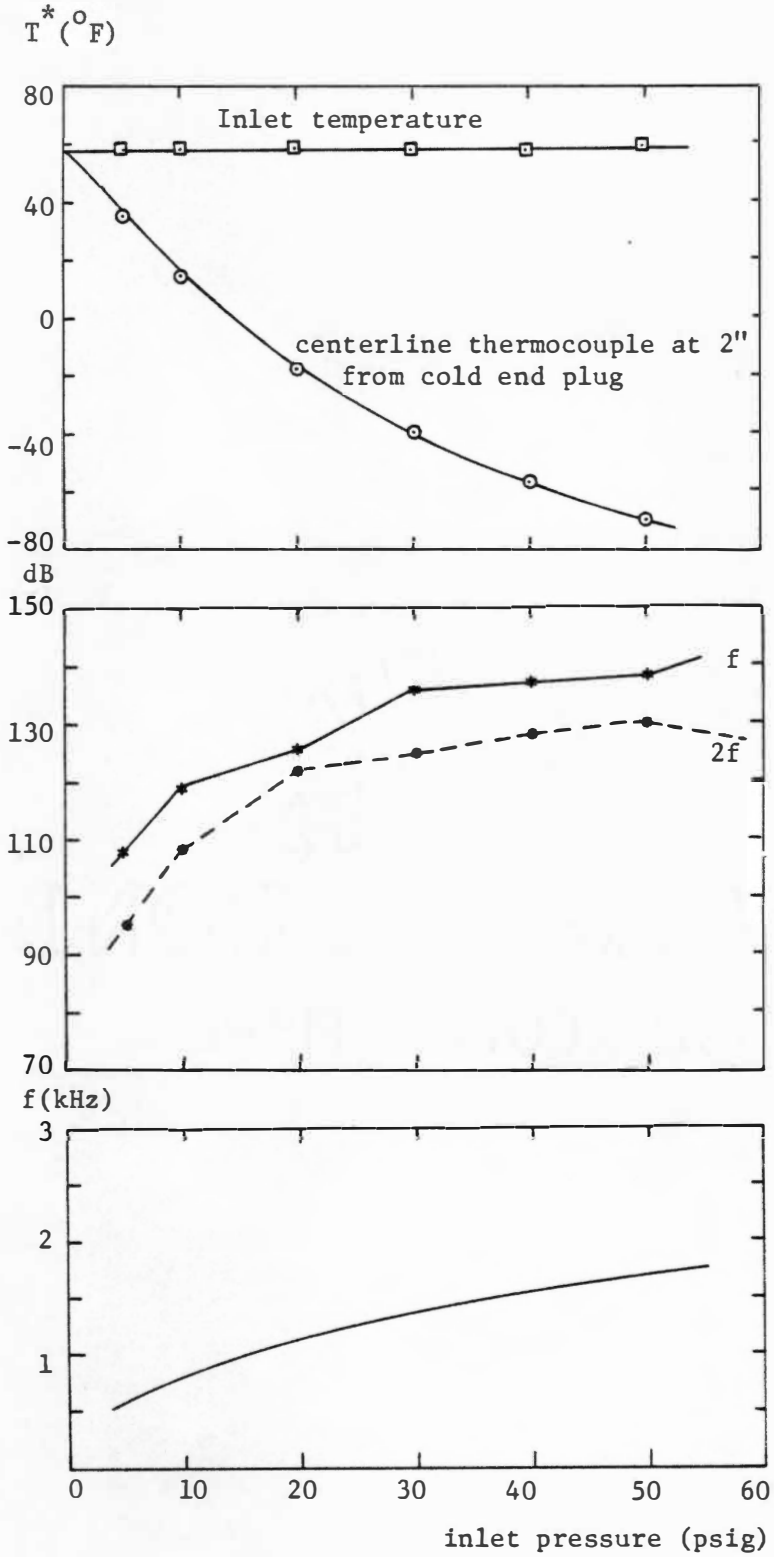

Figure 31. Data for zero acoustic cavity length.

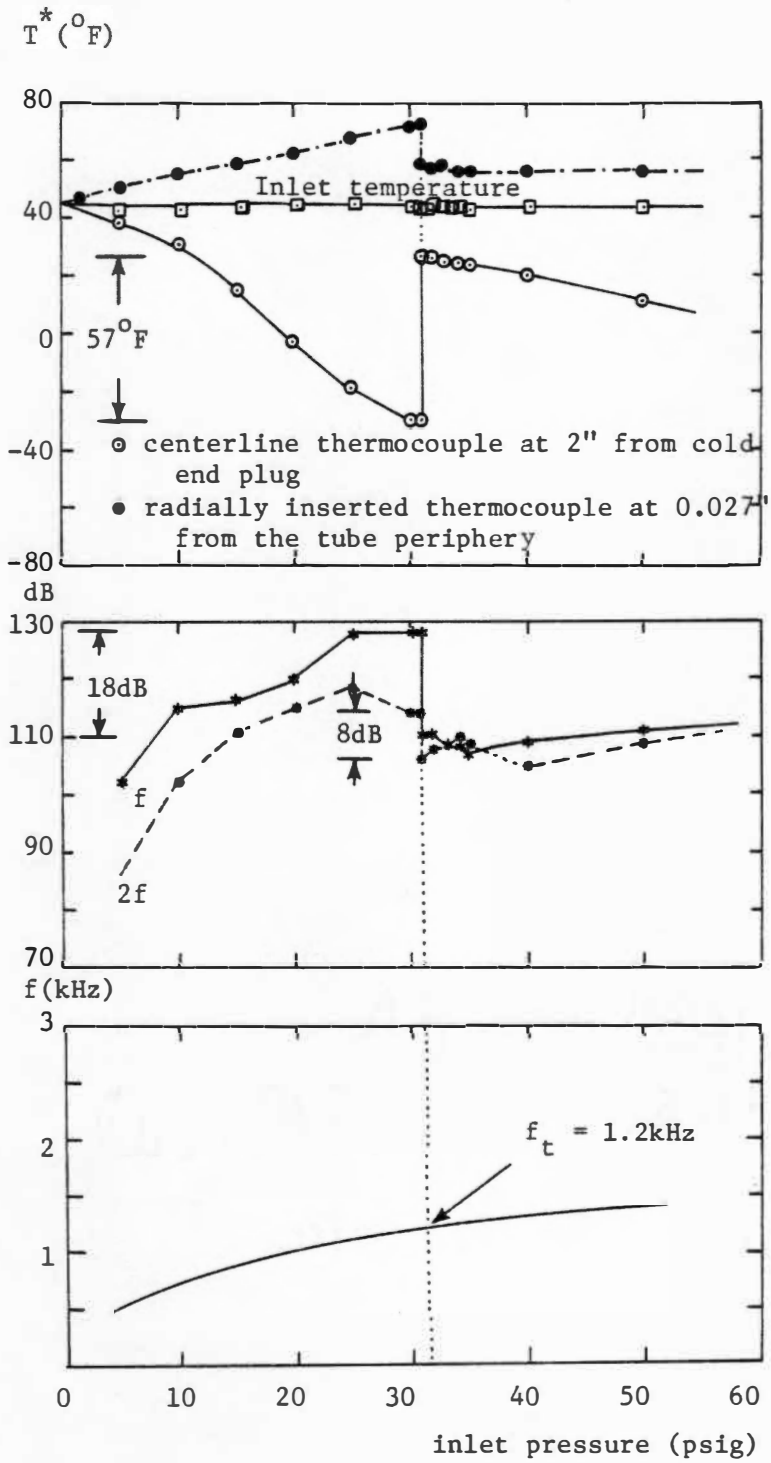

Figure 32. Data for 1.5 inch acoustic cavity length.

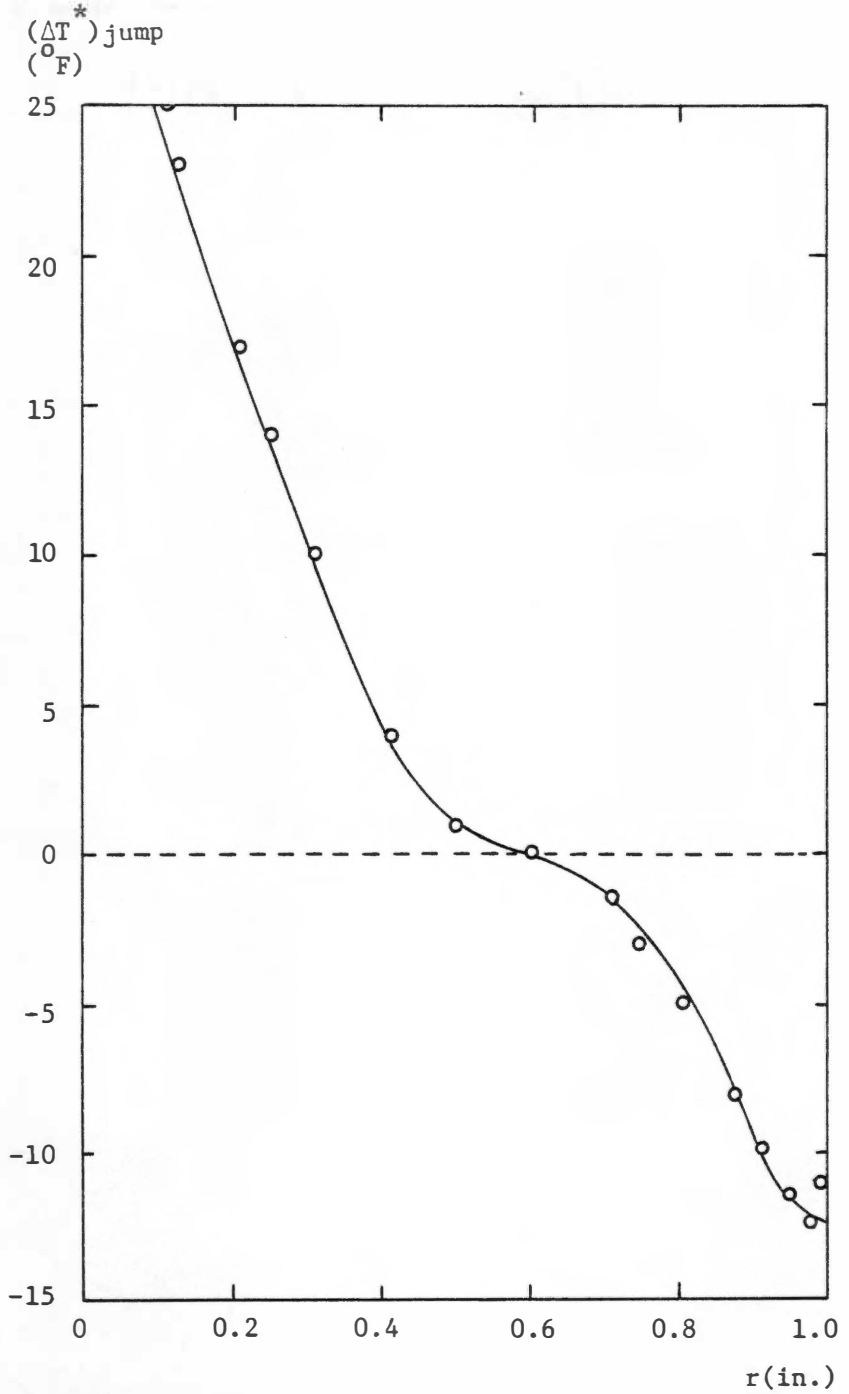

Figure 33. Radial variation of temperature jump at the tuned condition: axial position of radially inserted thermocouple at the eighteenth (18) acoustic cavity from the manifold end, 1.5 inch acoustic cavity length.

CHAPTER VI

CONCLUSION

It has been shown through the evidence presented herein, that the mechanism of the total temperature separation in the Ranque-Hilsch tube of the uniflow type is largely due to acoustic streaming induced by the vortex whistle – a spinning wave with a discrete frequency in swirling flows: near the periphery of a vortex tube, the induced d.c. tangential velocity adds to, and increase the steady swirl. At any swirl velocity, this deforms the base Rankine vortex into a forced vortex and leads to the total temperature separation in the radial direction.

BIBLIOGRAPHY

BIBLIOGRAPHY

1. Ranque, G. "Experiments on Expansion in a Vortex with Simultaneous Exhaust of Hot Air and Cold Air," Le Journal de Physique et Le Radium, 4 (Series 7, No. 6): 112S - 115S, 1933.

2. Hilsch, R. "The Use of Expansion of Gases in a Centrifugal Field as Cooling Process," The Review of Scientific Instruments, 18 (No. 2): 108 - 113, 1947.

3. Liepmann, H. W. and A. Roshko. Elements of Gasdynamics. New York: John Wiley and Sons, 1957. P. 170.

4. Van Deemter, J. J. "On the Theory of the Ranque-Hilsch Cooling Effect," Applied Scientific Research, 3 (Section A): 174 - 196, 1952.

5. Deissler, R. G. and M. Perlmutter. "Analysis of the Flow and Energy Separation in a Turbulent Vortex," International Journal of Heat and Mass Transfer, 1: 173 - 191, 1960.

6. Linderstrom - Lang, C. U. "The Three-dimensional Distribution of Tangential Velocity and Total Temperature in Vortex Tubes," Journal of Fluid Mechanics, 45 (Part 1): 161 - 187, 1971.

7. Hartnett, J. P. and E. R. G. Eckert. "Experimental Study of the Velocity and Temperature Distribution in a High Velocity Vortex Type Flow," Transactions of ASME, Journal of Heat Transfer, 79: 751 - 758, 1957.

8. Keyes, J. J., Jr. "Experimental Study of Flow and Separation in Vortex Tubes with Application to Gaseous Fission Heating," American Rocket Society Journal, 31 (No. 9): 1204 - 1210, 1961.

9. Lay, J. E., "An Experimental and Analytical Study of Vortex-Flow Temperature Separation by Superposition of Spiral and Axial Flows, Part 1," Transactions of ASME, Journal of Heat Transfer, 81 (Series C): 202 - 212, 1959.

10. Reynolds, A. "A Note on Vortex-tube Flows," Journal of Fluid Mechanics, 14 (Part 1): 18 - 20, 1962.

11. Savino, J. M. and R. G. Ragsdale. "Some Temperature and Pressure Measurements in Confined Vortex Fields," Transactions of ASME, Journal of Heat Transfer, 83 (Series C): 33 - 38, 1961.

12. Scheller, W. A. and G. M. Brown. "The Ranque-Hilsch Vortex Tube," Industrial and Engineering Chemistry, 49 (No. 6): 1013 - 1016, 1957.

13. Takahama, H. "Studies on Vortex Tubes," Bulletin of JSME, 8 (No. 31): 431 - 440, 1965.

14. Bruun, H. H. "Experimental Investigation of the Energy Separation in Vortex Tubes," Journal of Mechanical Engineering Science, 11 (No. 6): 567 - 582, 1969.

15. Sulbukin, M. "Unsteady, Viscous, Circular Flow Part 3. Application to the Ranque-Hilsch Vortex Tube," Journal of Fluid Mechanics, 72 (Part 2): 269 - 293, 1962.

16. Batson, J. L. and R. H. Sforzini. "Swirling Flow Through a Nozzle," Journal of Spacecraft and Rocket, 7 (No. 2): 159 - 163, February, 1970.

17. Scheper, G. W., Jr. "Vortex Tube - Internal Flow Data and Heat Transfer Theory," Refrigerating Engineering, 59 (No. 10): 985 - 989, October 1951.

18. McGee, R., Jr. "Fluid Action in the Vortex Tube," Refrigerating Engineering, 58 (No. 10): 974 - 975, October 1950.

19. Kendall, J. M. "Experiment Study of a Compressible Viscous Vortex," Technical Report No. 32-290, Jet Propulsion Laboratory, California Institute of Technology, Pasadena, California, 1962.

20. Ragsdale, R. G. "Applicability Mixing Length Theory to a Turbulence Vortex System," NASA TN D-1051, August 1961.

21. Syred, N. and J. M. Beer. "Vortex Core Precession in High Swirl Flows," Report No. FTCE/62/NS/72, Department of Chemical Engineering, Sheffield University, Sheffield, England, 1972.

22. Sprenger, H. "Beobachten and Wirbelrohren," Zeitschrift für Angewandte Mathematik und Physik, 2: 293 - 300, 1951.

23. Sprenger, H. S. "Über Thermische Effekte bei Rezonanzrohren," Mitteilungen aus dem Institut für Aerodynamik an der E.T.H., 21: 18 - 35, 1954.

24. Danforth, C. E. A private communication, 1977.

25. Rakowski, W. J., D. H. Ellis and H. R. Bankhead. "Research Program for the Experimental Analysis of Blade Stability," AIAA Paper, 78-1089, Las Vegas, NV, 1978.

26. Rakowski, W. J. and D. H. Ellis. "Experimental Analysis of Blade Instability - Interim Technical Report, Vol. 1, Phase II - Test Rig Checkout," R78 AEG 275, General Electric Company Report for F33615-76-C-2035, to Air Force Aero Propulsion Laboratory, WPAFB: 67-71, 1978.

27. Bennett, W. A. and M. C. Miller. "Experimental Evaluation of the AGT-100 Interturbine Duct/Collector Scroll Assembly," EDR 10573, Detroit Diesel Allison, Indianapolis, Indiana, May 1981.

28. Lighthill, M. J. "Acoustic Streaming," Journal of Sound and Vibration, 61 (No. 3): 391 - 418, 1978.

29. Vonnegut, B. "A Vortex Whistle," Journal of Acoustical Society of America, 26 (No.1): 18 - 20, 1954.

30. Vonnegut, B. "Vortex Thermometer for Measuring True Air Temperatures and True Air Speeds in Flight," Review of Scientific Instruments, 21 (No. 2): 136 - 141, 1950.

31. Nichlas, J. P. "Investigation of a Vortex Tube Acoustic True Airspeed Sensor," Cornell Aeronautical Laboratory Report No. IH-942-0-2, 1957.

32. Rodely, A. E., A. C. Chanaud and D. F. White. "A Digital Flowmeter Without Moving Parts," ASME Paper No. 65 - WA/Ftt-6, presented at ASME Winter Annual Meeting, Chicago, Illinois, 1965.

33. Lighthill, M. J. Wave in Fluids. Cambridge, England: University Press, 1978.

34. Andrade, E. N. da C. "On the Circulations Caused by the Vibrations of Air in a Tube," Proceedings of Royal Society, 134 (Series A): 445 - 470, 1932.

35. Schlichting, H. Boundary-Layer Theory. New York: McGraw-Hill Book Company, Inc., 1979.

36. Swithenbank, J. and G. Sotter. "Vortex Generation in Solid Propellant Rocket," AIAA Journal, 2(No. 7): 1297 - 1302, 1964.

37. Flandro, G. A. "Rotating Flows in Acoustically Unstable Rocket Motors," Ph.D. Thesis, California Institute of Technology, Pasedena, California, 1967.

38. Secomb, T. W. "Flows in a Channel with Pulsating Walls," Journal of Fluid Mechanics, 88 (Part 2): 273 - 288, 1978.

39. Kurosaka, M. "Acoustic Streaming in Swirling Flow and the Ranque-Hilsch Effect," Journal of Fluid Mechanics (in print).

40. Chanaud, R. C. "Experiments Concerning the Vortex Whistle," Journal of the Acoustic Society of America, 35: 953 - 960, 1963.

41. Chanaud, R. C. "Observations of Oscillatory Motion in Certain Swirling Flows," Journal of Fluid Mechanics, 21 (Part 1): 111 - 127, 1965.

42. Kelvin, Lord (W. J. Thompson). "Vibrations of a Columnar Vortex," Mathematical and Physical Paper. Vol. IV. Cambridge, England: Hydrodynamics and General Dynamics, 1910, Pp. 152 - 165.

APPENDICES

APPENDIX A

DIFFERENCE BETWEEN THE RANQUE-HILSCH EFFECT AND THE JOULE-THOMSON EFFECT

By throttling through a porous plug or globe valve, Joule and Thomson found that temperature of a gas can either rise or drop due to expansion or compression caused by the pressure gradient in the flow. The Joule-Thomson coefficient is given by:

$$\alpha_H = \frac{\partial T}{\partial p}|_{h=\text{constant}} .$$

If $\alpha_H > 0$, temperature drops due to expansion, while $\alpha_H < 0$, temperature rises due to compression.

Here it is demonstrated that one cannot use the Joule-Thomson effect to explain the Ranque-Hilsch effect.

Consider the flow in the Ranque-Hilsch tube with the following typical conditions:

- Inlet temperature $T_1 = 25^oC(298^oK), p_1 = 2$ atm. absolute (1 atm. gauge).

- Centerline temperature $T_2 = 0^oC(273^oK), p_1 = 2$ atm. absolute (0 atm. gauge).

For air, for example, in this temperature and pressure range, the Joule-Thomson coefficient $\alpha_H = 0.276(\frac{273}{T})^2\ ^oC/\text{atm.}$ and ΔT due to the Joule-Thomson effect is given by

$$\Delta T = \alpha_H \Delta p = 0.276\left(\frac{273}{T}\right)^2 \Delta p = 0.23^oC$$

where T is steady state temperature in ^{o}K and Δp the pressure difference while in the Ranque-Hilsch tube, $\Delta T = T_1 - T_2 = 25^{o}C$.

Thus the phenomenon of thermal energy separation in the vortex flow cannot be explained by the Joule-Thomson effect for the temperature difference obtained in the Ranque-Hilsch tube is by far larger.

APPENDIX B

DERIVATIONS OF THE TOTAL TEMPERATURE

Supposing the fluid to be nonviscous, non-heat conducting and unsteady, the general three-dimensional equations of motion can be described in terms of cartesian coordinates, as given by:

Continuity:

$$\frac{\partial \rho}{\partial t} + \frac{\partial}{\partial x_j}(\rho u_j) = 0 \qquad (B-1)$$

Momentum:

$$\frac{\partial}{\partial t}(\rho u_i) + \frac{\partial}{\partial x_j}(\rho u_i u_j) = -\frac{\partial p}{\partial x_i} + \rho f_i \qquad (B-2)$$

Energy:

$$\frac{\partial}{\partial t}(\rho e + \frac{1}{2}\rho u^2) + \frac{\partial}{\partial x_j}\left[(\rho e + \frac{1}{2}\rho u^2)u_j\right] = \rho q + \rho f_i u_i - \frac{\partial}{\partial x_i}(p u_i) \qquad (B-3)$$

where ρ and p are the density and pressure of the fluid, f_i and q the force and rate of heat addition per unit mass, e the internal energy.

Multiplying Eq. (B-1) by $(e + \frac{1}{2}u^2)$ and then substracting from Eq. (B-3), leads to

$$\rho \frac{De}{Dt} + \rho \frac{D}{Dt}\left(\frac{1}{2}u^2\right) = \rho q + \rho f_i u_i - \frac{\partial}{\partial x_i}(p u_i) \qquad (B-4)$$

where

$$\frac{D}{Dt} = \frac{\partial}{\partial t} + u_k \frac{\partial}{\partial x_k}$$

$$u^2 = u_1^2 + u_2^2 + u_3^2 = u_i u_i \ .$$

Rewriting the pressure term in the form

$$-\frac{\partial}{\partial x_i}(p u_i) = \frac{\partial p}{\partial t} - \rho \frac{D}{Dt}\left(\frac{p}{\rho}\right) \qquad (B-5)$$

with the help of the continuity equation. Substituting Eq. (B-5) into Eq. (B-4) and dividing through by ρ gives

$$\frac{D}{Dt}\left(e+\frac{p}{\rho}+\frac{1}{2}u^2\right)=q+f_iu_i+\frac{1}{\rho}\frac{\partial p}{\partial t}\ .$$

Introducing the total enthalpy, $h^*=e+\frac{p}{\rho}+\frac{1}{2}u^2$, the result is

$$\frac{Dh^*}{Dt}=q+f_iu_i+\frac{1}{\rho}\frac{\partial p}{\partial t} \qquad (B-6)$$

For a perfect gas, $h^*=C_pT^*$, Eq. (B-6) becomes

$$C_p\frac{DT^*}{Dt}=q+f_iu_i+\frac{1}{\rho}\frac{\partial p}{\partial t} \qquad (B-7)$$

where $T^*=T+\frac{1}{2}\frac{u^2}{C_p}$, the total temperature.

In the absence of any appreciable heat conduction, viscous dissipation and external work, the material derivative of total temperature can be expressed as:

$$C_p\frac{DT^*}{Dt}=\frac{1}{\rho}\frac{\partial p}{\partial t}\ . \qquad (B-8)$$

APPENDIX C

VISCOUS AND CONVECTION TERMS FOR ACOUSTIC STREAMING

In this appendix, it is shown that the viscous terms are as equally important as the convection terms for acoustic streaming.

To understand these important terms, consider the unsteady boundary layer. The flow is assumed to be two-dimensional incompressible for the purpose of exposition. Suppose that u_1 and U_1 are the real sinusoidally - varying velocities relative to the boundary, inside and just outside the boundary layer, respectively, as determined by the linear theory, that means

$$\frac{\partial u_1}{\partial t} = -\frac{1}{\rho}\frac{\partial p}{\partial x} + \nu\frac{\partial^2 u_1}{\partial x^2}$$
$$\frac{\partial U_1}{\partial t} = -\frac{1}{\rho}\frac{\partial p}{\partial x}$$

where U_1 is usually given and that $u_1 + u_2$ and $U_1 + U_2$ satisfy the complete non-linear equations which apply inside and just outside the boundary respectively, or

$$\frac{\partial(u_1+u_2)}{\partial t} + (u_1+u_2)\frac{\partial(u_1+u_2)}{\partial x} + (v_1+v_2)\frac{\partial(u_1+u_2)}{\partial y} = -\frac{1}{\rho}\frac{\partial p}{\partial x}$$
$$+\nu\frac{\partial^2(u_1+u_2)}{\partial x^2}$$
$$\frac{\partial(U_1+U_2)}{\partial t} + (U_1+U_2)\frac{\partial(U_1+U_2)}{\partial x} = -\frac{1}{\rho}\frac{\partial p}{\partial x} \quad .$$

Then since $|u_2|$ and $|U_2|$ are presumably small compared with $|u_1|$ and $|U_1|$, the equation for u_2 is approximately

$$\frac{\partial u_2}{\partial t} - \nu\frac{\partial^2 u_2}{\partial y^2} - \frac{\partial U_2}{\partial t} = U_1\frac{\partial U_1}{\partial x} - u_1\frac{\partial u_1}{\partial x} - v_1\frac{\partial u_1}{\partial y} \quad .$$

The expressions for u_2 and U_2 evidently consist of terms proportional to $\sin 2\omega t$ and to $\cos 2\omega t$ and of constant terms. The latter represent acoustic streaming under consideration, and the temporal average of all terms in the above equation gives

$$\nu \frac{\partial^2 \overline{u}_2}{\partial y^2} = \frac{\partial}{\partial x}\left(\frac{\overline{U}_1^2}{2}\right) - \frac{\partial}{\partial x}\left(\frac{\overline{u}_1^2}{2}\right) - \overline{v_1 \frac{\partial u_1}{\partial y}} \quad .$$

From this expression, for the generation of acoustic streaming $\overline{u}_2$, one recognizes the importance of both the viscous and nonlinear terms, appearing on both sides of the equations.

APPENDIX D

DISTURBANCE FREQUENCY IN INCOMPRESSIBLE FLOW

Consider a swirling flow in the cylinder length, L. Supposing the fluid to be homogeneous incompressible and unsteady, the effect of viscosity and heat conduction will be neglected. Let u_r, u_θ, u_z be the radial, angular, and axial velocities of the fluid; ρ and p the density and pressure of the fluid, and r the radial position of a fluid element. The continuity and momentum equations, in term of cylindrical coordinates, can then be written as:

$$\frac{1}{r}\frac{\partial}{\partial r}(ru_r)+\frac{1}{r}\frac{\partial u_\theta}{\partial \theta}+\frac{\partial u_z}{\partial z}=0$$

$$\frac{\partial u_r}{\partial t}+u_r\frac{\partial u_r}{\partial r}+\frac{u_\theta}{r}\frac{\partial u_r}{\partial \theta}+u_z\frac{\partial u_r}{\partial z}-\frac{u_\theta^2}{r}=-\frac{\partial}{\partial r}\left(\frac{p}{\rho}\right)$$

$$\frac{\partial u_\theta}{\partial t}+u_r\frac{\partial u_\theta}{\partial r}+\frac{u_\theta}{r}\frac{\partial u_\theta}{\partial \theta}+u_z\frac{\partial u_\theta}{\partial z}+\frac{u_r u_\theta}{r}=-\frac{1}{r}\frac{\partial}{\partial \theta}\left(\frac{p}{\rho}\right) \qquad (D-1)$$

$$\frac{\partial u_z}{\partial t}+u_r\frac{\partial u_z}{\partial r}+\frac{u_\theta}{r}\frac{\partial u_z}{\partial \theta}+u_z\frac{\partial u_z}{\partial z}=-\frac{\partial}{\partial z}\left(\frac{p}{\rho}\right)\ .$$

Each of the quantities is now expressed as the sum of a steady-state component, which is assumed to be a function of r only, and an unsteady small perturbation component, as given by

$$\begin{aligned} u_r &= \tilde{u}(r)\cos kz\sin(\omega t-m\theta)\\ u_\theta &= V(r)+\tilde{v}(r)\cos kz\cos(\omega t-m\theta)\\ u_z &= \tilde{w}(r)\sin kz\sin(\omega t-m\theta)\\ \frac{p}{\rho} &= F(r)+\overline{p}(r)\cos kz\cos(\omega t-m\theta) \end{aligned} \qquad (D-2)$$

with $F(r)=\int\frac{V^2(r)}{r}dr$.

Substituting the above transformations into Eq. (D-1) and neglecting squares and products of the infinitely small quantities, yields

$$\frac{d\tilde{u}}{dr} + \frac{\tilde{u}}{r} + \frac{m}{r}\tilde{v} + k\tilde{w} = 0 \qquad (D-3a)$$

$$-\frac{d\overline{p}}{dr} = \left(\omega - m\frac{V}{r}\right)\tilde{u} - 2\frac{V}{r}\tilde{v} \qquad (D-3b)$$

$$-m\frac{\overline{p}}{r} = \left(\frac{V}{r} + \frac{dV}{dr}\right)\tilde{u} - \left(\omega - m\frac{V}{r}\right)\tilde{v} \qquad (D-3c)$$

$$k\overline{p} = \left(\omega - m\frac{V}{r}\right)\tilde{w} \ . \qquad (D-3d)$$

Eliminating $\overline{p}$ and resolving for $\tilde{u}, \tilde{v}$ from Eq. (D-3), leads to

$$\tilde{u} = \frac{1}{kE}\left(\omega - m\frac{V}{r}\right)\left[\left(\omega - m\frac{V}{r}\right)\frac{d\tilde{w}}{dr} - \frac{m}{r}\left(\frac{V}{r} + \frac{dV}{dr}\right)\tilde{w}\right] \qquad (D-4)$$

$$\begin{aligned}\tilde{v} = {} & \frac{1}{kE}\left[\left(\frac{V}{r} + \frac{dV}{dr}\right)\left(\omega - m\frac{V}{r}\right)\frac{d\tilde{w}}{dr}\right] \\ & + \frac{1}{kE}\frac{m}{r}\left[\frac{V^2}{r} - \left(\frac{dV}{dr}\right)^2 - \left(\omega - m\frac{V}{r}\right)^2\right]\tilde{w}\end{aligned} \qquad (D-5)$$

where

$$E = \frac{2V}{r}\left(\frac{V}{r} + \frac{dV}{dr}\right) - \left(\omega - m\frac{V}{r}\right)^2 \ .$$

If it is assumed that the base swirling flow is of the Rankine vortex type; that is

$$\begin{aligned} V(r) &= \Omega r \ , \qquad 0 < r < r_i \\ &= \frac{\Gamma}{r} \ , \qquad r_i < r < r_o \end{aligned} \qquad (D-6)$$

where $\Gamma = \Omega r_i^2$, r_i denotes the radius at the interface between a forced and free vortex, r_o the radius of the tube, then it simplifies Eqs. (D-4) and (D-5) to

for $0 < r < r_i$

$$\tilde{u} = \frac{1}{kE}(\omega - m\Omega)\left[(\omega - m\Omega)\frac{d\tilde{w}}{dr} - 2\frac{m\Omega}{r}\tilde{w}\right]$$
$$\tilde{v} = \frac{1}{kE}(\omega - m\Omega)\left[2\Omega\frac{d\tilde{w}}{dr} - \frac{m}{r}(\omega - m\Omega)\tilde{w}\right] \qquad (D-7)$$

where $E = 4\Omega^2 - (\omega - m\Omega)^2$

and for $r_i < r < r_o$

$$\tilde{u} = -\frac{1}{k}\frac{d\tilde{w}}{dr}$$
$$\tilde{v} = \frac{m}{r}\frac{\tilde{w}}{k} \qquad (D-8)$$

and the elimination of $\tilde{u}$ and $\tilde{v}$ by these from Eq. (D-3a) gives

$$\frac{d^2\tilde{w}}{dr^2} + \frac{1}{r}\frac{d\tilde{w}}{dr} - \left(\frac{m^2}{r^2} - \nu^2\right)\tilde{w} = 0\,, \quad 0 < r < r_i \qquad (D-9)$$

$$\frac{d^2\tilde{w}}{dr^2} + \frac{1}{r}\frac{d\tilde{w}}{dr} - \left(\frac{m^2}{r^2} + k^2\right)\tilde{w} = 0\,, \quad r_i < r < r_o \qquad (D-10)$$

where

$$\nu^2 = k^2\frac{4\Omega^2 - (\omega - m\Omega)^2}{(\omega - m\Omega)^2}\,.$$

The solution of Eq. (D-9) has the form of

$$\tilde{w}_{\text{forced vortex}} = C' J_m(\nu r) + D' Y_m(\nu r) \qquad (D-11)$$

however, by the condition that $\tilde{w}$ is finite at $r = 0$, it reduces to

$$\tilde{w}_{\text{forced vortex}} = C' J_m(\nu r)\,. \qquad (D-12)$$

Similarly, the solution of Eq. (D-10) is

$$\tilde{w}_{\text{free vortex}} = A' I_m(kr) + B' Y_m(kr) \qquad (D-13)$$

where I_m, J_m and Y_m are the Bessel functions of order m; A', B', C', D' are constant.

$$\text{Boundary condition } \tilde{u} = 0 \qquad \text{at } r = r_o \tag{D - 14}$$

and the conditions to be fulfilled at the interface between the forced and free vortices are that $\tilde{u}(r)$ and $\overline{p}(r)$ must have the same values on the two sides of it; that means

$$\tilde{u}_{\text{forced vortex}} = \tilde{u}_{\text{free vortex}} \text{ at } r = r_i \tag{D - 15}$$

$$\overline{p}_{\text{forced vortex}} = \overline{p}_{\text{free vortex}} \text{ at } r = r_i \ . \tag{D - 16}$$

For the special case $k \to 0$ and hence $\nu \to 0$, using the asymptotic form of I_m, J_m and Y_m, yields

$$\tilde{w}_{\text{forced vortex}} = Cr^m \ , \quad 0 < r < r_i \tag{D - 17}$$

$$\tilde{w}_{\text{free vortex}} = Ar^m + Br^{-m} \ , \quad r_i < r < r_o \tag{D - 18}$$

then solving Eq. (D-14) and equating the condition in Eq. (D-16), yields

$$A = r_o^{-2m} B \tag{D - 19}$$

$$C = \left(r_o^{-2m} + r_i^{-2m}\right) B \ . \tag{D - 20}$$

Substituting Eqs. (D-17) and (D-18) into Eqs. (D-7) and (D-8), and applying the condition in Eq. (D-15), leads to

$$\omega = \left(m - 1 + \lambda^{-2m}\right)\Omega \tag{D - 21}$$

where $\lambda = \frac{r_o}{r_i}$.

APPENDIX E

STATIC TEMPERATURE FOR FORCED AND RANKINE VORTICES

If it is assumed that the entropy at the entrance is constant in the r-direction, then

$$\frac{p(r)}{(\rho(r))^2} = \text{constant in the } r\text{-direction} \qquad (E-1)$$

and

$$T(r) = T(r = r^*) + \frac{\gamma - 1}{\gamma R}\int_{r^*}^{r} \frac{1}{r} V^2(r) dr \qquad (E-2)$$

where r^* is the reference radius.

For a forced vortex

$$V(r) = \Omega_1 r \quad , \quad 0 < r < r_o$$

then

$$T(r) = T(r = r_o) + \frac{\gamma - 1}{2\gamma R}\Omega_1^2 (r^2 - r_o^2) \ . \qquad (E-3)$$

For a Rankine vortex

$$V(r) = \frac{\Gamma}{r} \quad , \quad r_i < r < r_o$$
$$= \Omega_2 r \quad , \quad 0 < r < r_i$$
$$\text{where } \Gamma = \Omega_2 r_i^2$$

then

$$T(r) = T(r = r_o) + \frac{\gamma - 1}{2\gamma R}\Gamma^2 \left(\frac{1}{r_o^2} - \frac{1}{r^2}\right) \ , \ r_i < r < r_o \qquad (E-4)$$

and

$$T(r) = T(r = r_o) + \frac{\gamma - 1}{2\gamma R}\Omega_2^2 \left(\frac{r_i^4}{r_o^2} - 2r_i^2 + r^2\right) \ , \ 0 < r < r_i \ . \qquad (E-5)$$

Thus, for $r_i < r < r_o$

$$\begin{aligned}\Delta T &= T(r)\text{Rankine} - T(r)\text{forced} \\ &= \frac{\gamma-1}{2\gamma R}\Gamma^2\left(\frac{1}{r_o^2}-\frac{1}{r^2}\right)+\frac{\gamma-1}{2\gamma R}\Omega_1^2(r_o^2-r^2) \\ &> 0 \quad \text{when} \quad \Omega_1 > \Omega_2 \\ &\text{or} \quad T(r)\text{Rankine} > T(r)\text{forced} \ .\end{aligned} \tag{E-6}$$

Similarly, for $0 < r < r_i$

$$\begin{aligned}\Delta T &= T(r)\text{Rankine} - T(r)\text{forced} \\ &= \frac{\gamma-1}{2\gamma R}\Omega_2^2\left(\frac{r_i^4}{r_o^2}-2r_i^2+r^2\right)+\frac{\gamma-1}{2\gamma R}\Omega_1^2(r_o^2-r^2) \\ &> 0 \quad \text{for} \quad \Omega_1 > \Omega_2 \\ &\text{or} \quad T(r)\text{Rankine} > T(r)\text{forced} \ .\end{aligned} \tag{E-7}$$

Therefore, the static temperature for a forced vortex is lower than the one for a Rankine vortex. In other words, at the tuned condition, the static temperature also rises because of the reversion from a forced vortex to a Rankine one.

VITA

Joseph Quang Chu was born in Phanrang, Ninhthuan, Vietnam, on May 27, 1955. He graduated from Vo Truong Toan High School, Saigon (Hochiminh City), Vietnam in June, 1973, and entered William Jennings Bryan College, Dayton, Tennessee in the Fall of 1974. With a major in Mathematics and Chemistry, he received a Bachelor of Arts degree in August, 1977.

He began graduate studies in September, 1977, at the University of Tennessee Space Institute, as a member of the Gas Dynamic Division. He subsequently received a Master of Science and a PhD degree with a major in Engineering Science in June, 1979, and December, 1982, respectively.

He is presently employed at Detroit Diesel Allison, Division of General Motors Corporation, in the Compressor Research and Design Section of the Reseach Department in Indianapolis, Indiana.

The author is a member of AIAA, ASME and Phi Kappa Phi.